



1 Quantifying the impact of synoptic weather types, patterns, 2 and trends on energy fluxes of a marginal snowpack

3 Andrew Schwartz¹, Hamish McGowan¹, Alison Theobald², Nik Callow³

4 ¹Atmospheric Observations Research Group, University of Queensland, Brisbane, 4072, Australia

5 ²Department of Environment and Science, Queensland Government, Brisbane, 4072, Australia

6 ³School of Agriculture and Environment, University of Western Australia, Perth, 6009, Australia

7

8 Correspondence to: Andrew J. Schwartz (Andrew.Schwartz@uq.edu.au)

9

10 Abstract.

11 Synoptic weather patterns and teleconnection relationships across a 39 year climatology are investigated for their
12 impact on energy fluxes driving ablation of a marginal snowpack in the Snowy Mountains, southeast Australia.
13 K-means clustering applied to ECMWF ERA-Interim data identified common synoptic types and patterns that
14 were then associated with in-situ snowpack energy flux measurements. The analysis showed that the largest
15 contribution of energy to the snowpack occurred immediately prior to the passage of cold fronts through increased
16 sensible heat flux as a result of warm air advection (WAA) ahead of the front. Indian Ocean Dipole and Southern
17 Oscillation Index phase combination had a strong relationship with energy flux, with eight of the ten highest
18 annual snowpack energy fluxes occurring during a negative IOD phase and positive SOI phase. Overall, seasonal
19 snowpack energy flux over the 39 year period had a decreasing trend that is likely due to a reduction in the number
20 of precipitation generating cold fronts and associated preceding WAA ahead of precipitation. This research is an
21 important step towards understanding changes in surface energy flux as a result of shifts to the global atmospheric
22 circulation as anthropogenic climate change continues.

23 1 Introduction

24 1.1 Synoptic weather influences on snow and glacier processes

25 Water generated in mountainous regions is a commodity that over 50% of the world's population depends on for
26 daily life (Beniston, 2003). Arguably, the most important role in the generation and regulation of these water
27 resources is that of montane snowpacks. These have been referred to as “water towers” (Viviroli et al., 2007) due
28 to their capabilities for storage and slow releases of meltwater. Many snowpacks are undergoing reductions in
29 spatial and temporal extent as a result of anthropogenic climate change (Pachauri et al., 2014). Understanding the
30 physical drivers of snowpack ablation, including synoptic-scale influences, is critical to help assess future water
31 resource availability in mountainous regions as climate change continues.

32 Snowfall has been related to synoptic weather types in numerous studies globally including in Athens (Prezerakos
33 and Angouridakis, 1984), the central and eastern United States (Goree and Younkin, 1966), the Tibetan Plateau
34 (Ueno, 2005), Budapest (Bednorz, 2008a), and the central European lowlands (Bednorz, 2011). However, work
35 on relationships between snowmelt and synoptic weather types is relatively scarce. Bednorz (2008b) identified
36 increased air temperature and rain-on-snow events as causes for rapid snowmelt ($> 5 \text{ cm day}^{-1}$) in the Polish-
37 German lowlands as a result of west-southwest airflows over Central Europe during positive phases of the North
38 Atlantic Oscillation (NAO). Similar work has been conducted in North America by Grundstein and Leathers
39 (1998) who were able to identify three main synoptic weather types responsible for significant snowmelt events
40 on the northern Great Plains, all of which included cyclonic influence with different low pressure centre locations



41 and warm air advection to the region. While some knowledge exists on synoptic drivers of snowpack ablation,
42 further research is needed to understand synoptic effects on ablation processes over snowpacks with varying
43 characteristics. Furthermore, research related to synoptic influences on the surface energy balance over marginal
44 snowpacks are rare. Hay and Fitzharris (1988) studied the influence of different synoptic weather types on glacier
45 ablation and snowpack melt, while Neale and Fitzharris (1997) used surface energy flux measurements to
46 determine which synoptic types resulted in highest ablation in the Southern Alps, New Zealand. These studies
47 found net radiation was the dominant term in ablation, but also noted that the contributions made by each term
48 varied largely depending on the synoptic type and its meteorology. A common characteristic between these studies
49 and others in various regions is that they focused primarily on the surface meteorology for synoptic classifications
50 rather than multiple level analysis, which enables insight to the potential influence of mid and upper-level
51 atmospheric conditions on surface – atmosphere energy exchanges. Regardless, no analysis at any level exists on
52 synoptic type influence on snowpack ablation within Australia.

53 **1.2 Synoptic weather types and trends in the Australian Alps**

54 Precipitation in the Australian Alps is crucial to agriculture, the generation of hydroelectric energy, and recreation
55 and was estimated to be worth \$9.6 billion per year in 2005 (Worboys and Good, 2011). A maximum in
56 precipitation in the Snowy Mountains typically occurs during the cooler months of June-September when it falls
57 as snow at elevations above 1400 m and accounts for twice as much precipitation as during the warmer periods
58 of the year (Chubb et al., 2011). While the snowpack of the Snowy Mountains typically exists for relatively short
59 periods compared to those of other regions where winter temperatures are lower and higher snowfall amounts
60 occur such as the European Alps and Rocky Mountains, USA, it is still a vital resource for southeast Australia
61 (SEA).

62 Synoptic weather types in Australia have been changing in recent decades in response to the impact of climate
63 change on background climate states (Hope et al., 2006; Theobald et al., 2016). For example, increases in daily
64 maximum temperature and reductions in precipitation during autumn and winter have been noted in SEA as a
65 result of anomalously high surface pressure during positive periods of the Southern Annular Mode (SAM)
66 (Hendon et al., 2007). Cai et al. (2005) also showed an increase in SAM value as a response to all global warming
67 experiments using the CSIRO Mark 3 climate model indicating a further poleward shift in the location of synoptic
68 systems. However, it has been suggested that the SAM accounts for a relatively small portion of seasonal rainfall
69 variability in Australia and other larger impacts on synoptic weather from other sources are likely (Meneghini et
70 al., 2007).

71 Rainfall in SEA is known to be influenced by the Southern Oscillation Index (SOI) and Indian Ocean Dipole
72 (IOD). Stone and Auliciems (1992) showed above (below) average rainfall amounts correspond to high (low) SOI
73 values through analysis using the k-means clustering technique. However, Pepler et al. (2014) identified IOD as
74 the dominant control on cool-season rainfall in SEA when compared to the El Nino Southern Oscillation (ENSO)
75 due to its effect on westerly wind patterns. In addition, positive IOD phases and associated shifts in synoptic types
76 have been identified as precursors to large bushfires in Austral spring and summer such as the Black Saturday and
77 Ash Wednesday events, two of the most severe fires in Australia's history, due to reductions in rainfall and soil
78 moisture (Cai et al., 2009a). Comparisons of the effects of IOD and ENSO phases on precipitation in SEA by
79 Ummenhofer et al. (2009) showed the positive phase of the IOD as the primary driver of large droughts as a result



80 of reduced moisture advection from the tropical seas northwest of Australia. The relationship between positive
81 IOD phase and reduction in rainfall for SEA is particularly concerning when climatological trends have noted an
82 increased likelihood of positive IOD periods as a result of climate change (Cai et al., 2009b).

83 **1.3 The Australian snowpack**

84 Characteristics of the snowpack in the Australian Alps have been examined in a number of studies with focus on
85 spatial and temporal snow cover variability (Budin, 1985; Duus, 1992), influence on catchment hydrology (Costin
86 and Gay, 1961), the energetics of snowpack melt (Bilish et al., 2018), and isotopic composition of precipitation
87 (Callow et al., 2014). Given observed declines in snow cover, climate change has become a central focus of this
88 research (Chubb et al., 2011; Hennessy et al., 2008; Nicholls, 2005; Reinfelds et al., 2014; Whetton et al., 1996)
89 as any changes to energy flux over the region will significantly impact the already marginal snowpack. Hennessy
90 et al. (2008) showed that future projections for the Australian snowpack predict reductions in annual areal snow
91 cover of 10-39% by 2020 and 22-85% by 2050. Observations indicate that reduction in snow cover is already
92 occurring with shortened annual periods of wintertime precipitation. Nicholls (2005) found reductions of 10%
93 and 40% in the maximum snow depth and snow depth at the first October measurement respectively from 1962
94 to 2002. In addition, wintertime precipitation was shown to have reduced by an average of 43% in high elevation
95 regions from 1990-2009 (Chubb et al., 2011), though much of this could have been due to several severe droughts
96 that occurred during the study period. Fiddes et al. (2015) showed that snowfall, snow accumulation, and snow
97 depth were highly correlated with temperature and that warming, as a result of climate change, could lead to
98 further reductions in the SEA snowpack. The importance of the water generated in the Australian Alps, reduction
99 in wintertime precipitation amounts and frequency, and high spatiotemporal variability of snow accumulation and
100 ablation (Budin, 1985) warrants an understanding of the energetics of Australia's snowpack as they pertain to the
101 influences of shifting synoptic-scale circulations.

102 Significant work has been conducted on identification of patterns and trends in Australian synoptic climatology
103 as it pertains to precipitation variability (Chubb et al., 2011; Pook et al., 2006; 2010; 2012, 2014; Theobald et al.,
104 2016). However, impacts on surface energy fluxes as a result of synoptic types and changing climatological
105 conditions have not been explored as they have in other regions. The objective of this study is to identify the
106 synoptic weather types that contribute the highest amounts of energy fluxes to the Australian snowpack, and their
107 climatological trends. This is accomplished through: 1) the identification and classification of common synoptic
108 types during periods of homogeneous snow cover, 2) attribution of snowpack energy flux characteristics to each
109 synoptic type, 3) construction of energy balance patterns as they pertain to common synoptic
110 patterns/progressions, and 4) investigation of relationships between trends in snowpack energy flux and
111 teleconnections.

112 **2 Methods**

113 **2.1 Study site and climate**

114 Energy flux measurements were made 16 km west of Lake Jindabyne at the Pipers Creek catchment headwaters
115 (36.417°S, 148.422°E) at an elevation of 1828 m in the Snowy Mountains, Kosciuszko National Park, New South
116 Wales (NSW), Australia (Figure 1). The catchment is classified as sub-alpine and contains grasslands, sub-alpine
117 bogs, and sub-alpine woodland (Gellie, 2005). The surrounding areas contain a mixture of living and dead
118 *Eucalyptus pauciflora* (Snow Gum) trees and open grassland areas with fens and alpine bogs. Many of the Snow



119 Gums were impacted by fire in 2003, and have experienced slow regrowth. The area's mixed characteristics of
120 forested and open grasslands with alpine wetlands within the Pipers Creek study catchment and immediately
121 surrounding the flux tower site are representative of those found throughout the Australian Alps.

122 The Snowy Mountains are characterized by relatively mild weather conditions compared to other mountain
123 ranges. Winter temperatures are typically around 0°C with mean low temperatures during July (the coldest month)
124 at -5°C and mean high temperatures between 2-4°C (Bureau of Meteorology, 2018b) that readily allow for melt
125 of the snowpack. Precipitation reaches a peak during the winter and spring months with the majority falling as
126 snow during July and August before ablating completely in late spring or early summer. Prevailing winds in the
127 region are westerly and reach a maximum in intensity during September and October, but intense wind events are
128 common throughout winter and spring during the passage of cold fronts. Snowpack properties in the catchment
129 are consistent with those of maritime snowpacks that are associated with basal melting, high temperatures, and
130 high wind speeds (Bilish et al., 2018; Sturm et al., 1995).

131 **2.2 Instrumentation**

132 An energy balance site (Figure 2) was installed in the Pipers Creek catchment headwaters on June 10th of 2016.
133 The site consists of a Campbell Scientific eddy covariance system to measure fluxes of latent and sensible heat at
134 10 Hz at a height of 3.0 m above ground level (AGL). A Kipp and Zonen CNR4 radiometer (3.0 m AGL) was
135 used to measure incoming and outgoing shortwave and longwave radiation to allow for comparisons of all
136 radiation components rather than simply net all-wave radiation. Ambient air temperature and relative humidity
137 were measured at the top of the mast by a Vaisala HMP155 probe at ~3.1 m above ground level. A Hukseflux
138 heat flux plate measured ground heat flux at a depth of 5 cm and was placed approximately 0.5 m from the centre
139 of the mast to minimize any influence the mast could have on snow accumulation above the sensor. Surface
140 temperatures were monitored using an Apogee Instruments SI-111 infrared radiometer at approximately 2 m from
141 the centre of the mast. Details on the instruments used for each measurement are shown in Table 1.

142 The eddy covariance system was controlled by a Campbell Scientific CR3000 micrologger with raw 10 Hz data
143 stored on memory cards at the site to allow for in-depth analysis of data as a back-up to the 30-minute averages
144 that were also recorded. In addition, data tables were recorded that contained notes for all measurements to allow
145 for potential identification of problematic measurements in real-time and analysis. All data was monitored in near-
146 real time through download of telemetered data with the exception of the 10 Hz tables that were collected through
147 replacement of the micrologger memory cards approximately every four months.

148 Precipitation data from an ETI Instrument Systems NOAH II weighing gauge located approximately 1 km to the
149 northwest of the energy balance site at elevation of 1761 m was supplied by Snowy Hydro Limited (SHL). A 6 m
150 diameter DFIR shield was used around the gauge in order to prevent wind-related under-catch of snowfall
151 (Rasmussen et al., 2012), and was additionally sheltered by vegetation to the west.

152 **2.3 Identification of snow cover periods**

153 Homogeneous snow cover is crucial to accurate measurement and analysis of snowpack energy balance (Reba et
154 al., 2009). Periods with homogeneous snow cover were determined using data from the Pipers Creek
155 instrumentation site and were cross referenced to manual snow measurements made at the Spencers Creek Snow
156 Course 6.6 km northwest of the Pipers Creek field site (Snowy Hydro Ltd, 2018). Periods with surface



157 temperatures above 1.5°C as measured by the SI-111 infrared radiometer that did not correspond to rain-on-snow
158 events and periods with albedo measurements less than 0.40 (Robock, 1980) were considered not to have
159 heterogeneous snow cover and were eliminated.

160 **2.4 Synoptic classification of snow cover days**

161 Synoptic weather type classification of homogeneous snow cover days was conducted using synoptic typing
162 methods adapted from Theobald et al. (2015). European Centre for Medium-Range Weather Forecasts (ECMWF)
163 ERA-Interim reanalysis data (Dee et al., 2011) with a 0.75° X 0.75° resolution was obtained for each day from
164 June 10th, 2016 through October 31st, 2017. This date range was chosen to ensure inclusion of all potential dates
165 with snow cover during the 2016 and 2017 snow seasons after the initial instrument tower installation on June
166 10th, 2016. Variables included in the reanalysis data consisted of mean daily values of Mean Sea Level Pressure
167 (MSLP); temperature and relative humidity values at 850, 700, 500, and 250 hPa; wind vectors at 10 m AGL,
168 850, 700, 500, and 250hPa; and 1000-500 hPa geopotential heights. The domain of the included variables was
169 limited to 20°S - 46°S and 120°E -160°E, ensuring coverage of synoptic scale systems affecting the Australian
170 Alps.

171 Focus was placed on analysis of temperature (T_d) and relative humidity (RH) values because of their impact on
172 latent heat, sensible heat, and radiative fluxes (Allan et al., 1999; Reba et al., 2009; Ruckstuhl et al., 2007; Webb
173 et al., 1993). Relative humidity values at 850, 700, and 500 hPa were used to investigate the potential influence
174 of cloud cover. MSLP and wind vector analysis at the 850, 700, 500, and 250 hPa levels allowed for the
175 identification of T_d and RH advection (Pook et al., 2006) into the Australian Alps. Thickness between 1000-500
176 hPa was used to determine frontal positions relative to the Australian Alps (Pook et al., 2006) and accordingly the
177 Pipers Creek field site.

178 Days within the ERA-Interim data that matched snow cover days were extracted and analysed using the k-means
179 clustering algorithm developed by Theobald et al. (2015). The algorithm was tested for 1-20 clusters and an elbow
180 plot of the cluster distances was used to identify the optimum number of clusters (Theobald et al., 2015), which
181 was seven. The identification of an elbow in the plot (Figure 3) at seven clusters indicates a reduction to the benefit
182 of adding additional clusters as the sum of distances for additional clusters fails to yield significant reductions
183 beyond that point (Wilks, 2011).

184 Clustering of the synoptic conditions for each day was verified through manual analysis of MSLP and 500 hPa
185 charts from the Australian Bureau of Meteorology (BOM) (Bureau of Meteorology, 2018). Cloud cover for each
186 type was investigated and verified through the use of visible band Himawari-8 satellite data
187 (<https://www.ncdc.noaa.gov/gibbs/>) at 03:00 UTC (13:00 local time) with one of three categories assigned to each
188 day studied; 1) no cloud cover, 2) partial cloud cover, or 3) complete cloud cover. Cloud cover was investigated
189 at midday to avoid misclassification due to short-lived clouds that appear over the area during the dawn and dusk
190 periods.

191 Manual verification of the k-means clustering algorithm using BOM synoptic charts identified four days (2.33%)
192 out of the 172 classified during the 2016 and 2017 seasons that had been classified incorrectly and they were
193 subsequently moved to their correct synoptic type. Three of the four misclassified days were early (June 7th, 2016)
194 or late (September 19th and 22nd, 2016) in the snowpack seasons with the fourth occurring in the middle of winter



195 on July 31st of 2017. Synoptic characteristics from these days tended to be complicated with no discernible
196 dominant features that matched those of classified types. This is likely due to shifting synoptic conditions between
197 seasons related to poleward or equatorial shifts in westerly winds.

198 2.5 Snowpack energy accounting

199 Accurate measurement of snowpack energy balance and associated melt can be difficult due to snowpack
200 heterogeneity (Reba et al., 2009) and problems with energy balance closure (Helgason and Pomeroy, 2012). The
201 snowpack energy balance can be expressed as:

$$202 \quad Q_m = Q^* + Q_h + Q_e + Q_g + Q_r \quad (1)$$

203 where the energy available for snow melt (Q_m) is equal to the sum of net radiation exchange (Q^*), sensible (Q_h)
204 and latent (Q_e) heat flux, ground heat flux (Q_g), and the energy flux to the snowpack from liquid precipitation
205 (Q_r) (Male and Granger, 1981; McKay and Thurtell, 1978).

206 While net all-wave radiation exchange (Q^*) is used for basic analysis of the snowpack energy balance, a
207 decomposition into its individual components is necessary to understand the role of short and longwave radiation
208 exchange in snowpack energetics (Bilish et al., 2018). Therefore, net radiation should be broken into its net flux
209 terms:

$$210 \quad Q^* = K^* + L^* \quad (2)$$

211 that quantify the net shortwave (K^*) and net longwave (L^*) components.

212 The approach taken within this paper is to examine net radiative flux components individually, similar to the
213 methods used by Bilish et al. (2018), to be precise in the identification of synoptic-scale effects on snowpack
214 energy fluxes through differences in temperature, relative humidity, cloud cover. Q_m calculation and comparisons
215 of snowpack energy flux terms were performed using the terms in Eq. (1), but with the net radiation terms (K^* and
216 L^*) used rather than summed as net all-wave radiation (Q^*) only.

217 2.6 Energy flux measurements of synoptic types

218 Energy flux measurements made at the Pipers Creek tower underwent a series of measurement corrections prior
219 to analysis. Coordinate rotation based on the methods of Wilczak et al. (2001) was applied on the 10 Hz EC data
220 to remove levelling errors in sonic anemometer mounting when calculating fluxes. In addition, frequency
221 corrections were made to the EC data to account for sensor response delay, volume averaging, and the separation
222 distance of the sonic anemometer and gas analyser when calculating fluxes (Campbell Scientific, 2018b). Finally,
223 WPL air density corrections (Webb et al., 1980) were made by the software to account for vertical velocities that
224 exist as a result of changing air mass density through fluxes of heat and water vapour.

225 Q_h and Q_e flux were calculated using the EC equations of:

$$226 \quad Q_h = -\rho C_p (\overline{w'\theta'}) \quad (3)$$

$$227 \quad Q_e = -\rho L_v (\overline{w'q'}) \quad (4)$$



228 where ρ is air density (kg m^{-3}), C_p is the specific heat of air ($1005 \text{ J kg}^{-1} \text{ deg}^{-1}$), $\overline{w'\theta'}$ is the average covariance
229 between the vertical wind velocity w (ms^{-1}) and potential temperature θ (K), L_v is the latent heat of sublimation
230 or vaporization of water (J kg^{-1}), and $\overline{w'q'}$ is the average covariance between the vertical wind velocity w (ms^{-1})
231 and specific humidity q (kg kg^{-1}) (Reba et al., 2009).

232 The calculation of energy flux imparted to the snowpack from rainfall (Q_r) followed Bilish et al. (2018) and was
233 determined using three separate calculations to establish approximate wet bulb temperature (T_w) (Stull, 2011), the
234 fraction of precipitation falling as rain ($1 - P_{snow}$) (Michelson, 2004), and total rain flux (Q_r) based on
235 precipitation accumulation over a 30-minute period.

236 2.6.1 Energy flux data quality control

237 Data quality control was performed on the filtered energy flux data to remove potential erroneous data. Periods
238 were omitted from analysis where latent and/or sensible heat flux measurements were rated ≥ 7 by the Campbell
239 Scientific EasyFlux™ software indicating problems with non-stationarity of wind flow, turbulence characteristics,
240 or horizontal orientation of the sonic anemometer (Foken et al., 2012). Q_e and Q_h values were also removed when
241 water vapour signal strength from the gas analyser was < 0.70 in order to remove erroneous readings during
242 periods of precipitation (Campbell Scientific, 2018a; Gray et al., 2018). De-spiking was performed on sensible
243 and latent heat data by visual inspection and through the application of filtering techniques to remove erroneously
244 high or low values. Latent heat and sensible heat flux thresholds of -100 Wm^{-2} to 500 Wm^{-2} and -200 Wm^{-2} to 500
245 Wm^{-2} , respectively, were applied to remove erroneous values that had been identified during visual inspection. In
246 addition, a seven point moving-median filter was implemented over three iterations to remove values more than
247 3.0 standard deviations away from the median values.

248 Pre-existing gaps and gaps introduced into the data by the quality control procedures were filled using two
249 methods described by (Falge et al., 2001a; 2001b). Linear interpolation of missing Q_e and Q_h values was used for
250 gaps up to 90 minutes in length. Look-up tables using six categories of stability (ζ), five categories of wind speed
251 (u), five categories of relative humidity (RH), and six categories of the difference between surface and
252 atmospheric temperatures (dT) were used to fill any gaps longer than 90 minutes. Traditionally, mean diurnal
253 variation values are also used for gap filling procedures (Bilish et al., 2018; Falge et al., 2001a; 2001b). However,
254 it was determined that using mean values would likely obscure any unique energy balance characteristics of the
255 synoptic types being investigated and, therefore, was not included as a gap-fill strategy for the data.

256 Following quality control procedures, 3864 of the initial 12147 records (31.8%) remained in the Q_e data and 4540
257 records (37.4%) remained in the Q_h data. Linear interpolation yielded an addition of 1693 Q_e values (13.9%) and
258 1513 Q_h values (12.5%). Look-up tables were the largest source of gap-filled data with the contribution of an
259 additional 6480 Q_e values (53.3%) and 5991 Q_h values (49.3%). Root Mean Squared Error (RMSE) and Mean
260 Bias Error (MBE) were calculated for 100 iterations of the gap-fill process using values available following quality
261 control procedures. This resulted in mean RMSE values of 20.9 Wm^{-2} and 33.9 Wm^{-2} during the observation
262 period for Q_e and Q_h , respectively. Missing values still existed in the Q_e and Q_h data following the gap-filling
263 procedures, however, these values were less than 1% of the initial 12147 records.



264 This research uses the energy flux convention where positive values are flux to the snowpack and negative values
265 are flux away from the snowpack.

266 **2.7 Determining climatology of snowpack energy flux**

267 The Snowy Mountains snowpack at elevations similar to Pipers Creek (1828 m) generally exists from June
268 through the end of October though it may begin as early as late-April and exist into early December (Snowy Hydro
269 Ltd, 2018). However, for climatological comparisons of synoptic types and snowpack energy flux the period of
270 most-likely snow cover, June through October, will be considered as the snowpack/snow cover season as times
271 outside of this period are not consistent in their snow cover properties. This season has been used to minimize
272 error introduced into the analysis through the incorporation of periods without snow cover.

273 Following the identification of the optimum number of synoptic types and their corresponding energy flux
274 characteristics, each day between June 1st and October 31st from 1979 through 2017 (39 seasons) was classified
275 using the synoptic types developed from the 2016 and 2017 snow cover days. Each type was analysed for trends
276 in frequency over the 39 year period to develop a climatology of the synoptic types in the Snowy Mountains
277 region. Annual counts of each type were then determined and were multiplied by the mean daily net snowpack
278 energy flux for each synoptic type found during the 2016-2017 seasons. Mean daily flux values were then summed
279 for each year and trends in snowpack energy flux as it pertains to synoptic scale atmospheric conditions were
280 identified over the 39 year period. We acknowledge our results represent an estimate of the snowpack energy flux
281 over the 39 year record based on similar synoptic conditions observed during the observational campaign in 2016
282 and 2017.

283 Investigation into teleconnection impacts on synoptic types was conducted to determine impacts of the IOD, SAM,
284 and SOI phase on synoptic type occurrence. Monthly data for each of the teleconnections from 1979 to 2017 was
285 obtained from the National Oceanic and Atmospheric Administration's (NOAA) Earth System Research
286 Laboratory (ESRL) (<https://www.esrl.noaa.gov/psd/data/climateindices/list/>). Mean values for each synoptic type
287 were determined for each of the three indices and correlations were calculated between mean seasonal flux and
288 each index.

289 **3 Results**

290 Identification of homogeneous snow cover days for the 2016 and 2017 snow seasons (June – October) resulted in
291 172 total days with 90 days occurring in the 2016 and 82 days in 2017. July, August, and September had the
292 highest number of classifiable days during the period. June and October still had periods with homogenous snow
293 cover, but they became intermittent and fewer classifiable days were in each of the months. This led to fewer
294 periods of study at the beginning and end of the snow seasons when snowpack was variable, with more in the late
295 winter and early spring months when snow cover was more consistent. Mean surface, cloud, and energy flux
296 characteristics of synoptic types identified during the two seasons are presented in Table 2.

297 **3.1 Synoptic types**

298 **3.1.1 Surface characteristics**

299 The dominance of the subtropical ridge in Australia's mid-latitudes is evident in the synoptic types. Four of the
300 types (T1,T2,T5 and T7) display dominant surface high pressure systems, each with slightly different orientation
301 and pressure centre locations (Figure 4) resulting in different energy flux characteristics. Dominant south-



302 southwesterly winds from T1 are the result of the high pressure centre being located to the northwest of the study
303 area. T2 has a predominantly zonal flow resulting from an elongated high to the north-northeast. T5 and T7 are
304 characterized by north-northwesterly flow from high pressure centres over the New South Wales
305 (NSW)/Queensland (QLD) coast and directly over the Snowy Mountains region, respectively.

306 T3 is characterized as having dominant northwest winds along a trough axis that is positioned over SEA with a
307 secondary coastal trough extending from southern NSW to the NSW/QLD border. T4 shows a transition from a
308 surface trough that has moved to the east of the study region to a high pressure system that is moving into the area
309 with winds from both features that converge over the Snowy Mountains region. The only synoptic type to have
310 dominant influence from a surface low was T6 that had weak south-southwesterly flow over the region from a
311 weak cut-off low to the east. For the purposes of this research, the identification of cut-off lows follows the
312 characteristics outlined by Chubb et al. (2011) that omits the presence of a closed circulation, but includes a cold
313 anomaly aloft that was cut off from the westerly wind belt.

314 Several types (T1, T4, T5, & T6) are considered to be 'transition types' that exist as the region is switching
315 between dominant high or low pressure surface features. T1, T4, and T6 are post-frontal transition types that show
316 high pressure ridging into the region following the passage of a trough that has either moved to the east (T1 &
317 T4) or developed into a weak lee-side cut-off low (T6). T5 shows the approach of a trough from the west and an
318 associated transition to a low pressure system. T2 and T7 show the area under the influence of zonal flow as a
319 result of high pressure systems centred over the area, while T3 shows SEA under the influence of a trough at the
320 time of observations.

321 **3.1.2 Relative humidity and cloud cover**

322 Understanding RH values associated with different synoptic types provides the ability to track types that are
323 favourable for high Q_e exchange with the snowpack. In addition, RH values at all tropospheric levels can have
324 impacts on snowpack energy flux through influences on K and L exchange via changes to insolation and the
325 absorption and emission of L . The identification of RH characteristics and associated cloud cover is necessary to
326 fully develop energy flux characteristics for each type.

327 Many of the synoptic types display local RH maxima in the Snowy Mountains region at 850 hPa (Figure 5) and,
328 while T5 has the lowest RH values of all types, it still has slightly higher RH values over the area. The elevation
329 in RH values in the region is most likely caused by changes of air mass thermodynamic properties due to
330 orographic forcing of the mountains (Ahrens, 2012). T4 and T6 had the highest RH values over the region at 850
331 hPa with both being widespread and higher than 90%. T6 shows strong southerly advection of elevated RH values
332 from the tropics along the NSW and QLD coast ahead of troughs at 700 and 500 hPa (Figures 6 & 7) that are
333 associated with the surface cut-off low.

334 Manual identification of cloud cover agreed with the mean RH characteristics of T4 and T6 with both types having
335 100% cloud cover between partial and complete cloud cover days (Table 3). T6 showed the highest RH values of
336 any type with values greater than 90% over the region at the 700 and 500 hPa levels. While not definitive, this
337 would suggest that T6 has deeper or more cloud layers than T4, which likely only has clouds at lower altitudes.
338 T2 and T7 had the lowest percentage (both 76%) of days with any cloud cover, which is confirmed by their low
339 RH values at 700 hPa (<20% & <30%) and 500 hPa (<30% & <40%), respectively. In addition, they also had the



340 highest percentage of cloud-free days (both 23%). The remaining types (T1, T3, and T5) showed a relatively
341 consistent number of cloud days based on the satellite observations that were all above 85%.

342 **3.1.3 Temperature**

343 Temperature characteristics of synoptic types at low and mid-levels in the atmosphere are crucial to identify those
344 with the highest surface sensible heat flux characteristics. The highest mean temperatures and strongest warm air
345 advection (WAA) in the Snowy Mountains region at 850 hPa (Figure 8) was found to be from T5 that is driven
346 by converging winds on the back of a high pressure circulation to the east and the leading edge of a trough to the
347 west. T2 and T3 have the second and third highest temperatures, respectively, but have different advection
348 characteristics. T2 shows relatively weak WAA into the Snowy Mountains region associated with zonal flows at
349 850 hPa resulting from the high pressure circulations located to the north (similar to T7). However, T3 shows cold
350 air advection (CAA) from recent cold frontal passage with dominant winds from the west-northwest.

351 Overall, CAA at 850 hPa can be identified in four of the seven types (T1, T3, T4, and T6) and warm air advection
352 exists in the other three synoptic types (T2, T5, and T7). Of the four CAA types, T1 and T4 advection is being
353 generated through south-southwest and west-southwest winds, respectively, related to high pressure centres to the
354 northwest. Despite a stronger southerly component of dominant CAA winds in T1, temperatures are lower in T4
355 which has a higher westerly component to the wind. T6 shows CAA related to converging winds on the back of a
356 trough to the east and a high to the northwest.

357 **3.1.4 Frequency and duration**

358 The frequency of each synoptic type during the 2016 and 2017 snowpack seasons is shown in Table 4. T3 and T7
359 occurred most frequently with 26.74% (46 days) and 19.77% (34 days) respectively. The higher number of days
360 in T3 and T7 is reflected in the mean type duration that shows these types with the longest duration, which is
361 likely due to these synoptic types occurring in a more stagnant synoptic pattern over multiple days as seen in the
362 mean type duration (Table 2).

363 Transition probabilities for the 2016 and 2017 seasons were developed similar to those used by Kidson (2000)
364 that detail the likelihood of a synoptic type occurring on the following day given an initial type (Table 5). The
365 highest transition probabilities were identified for each type and a flowchart was developed based on the most
366 likely synoptic type progressions (Figure 9). If the highest transition probabilities were within < 0.05 of each
367 other, two paths were plotted. The flowchart shows what would be expected for a basic synoptic-scale circulation
368 at mid-latitudes; a trough propagating eastward into the Snowy Mountains region in T7, T5, and T3; either
369 continued eastward movement of the surface trough (T4) or the development of a weak cut-off low (T6); then
370 transitioning to dominant high pressure over the region again (T2, T1, or T7).

371 **3.2 Energy flux characteristics of synoptic types**

372 It is important to consider the effects of synoptic type frequency when determining primary sources of energy
373 fluxes over long periods as synoptic types that contribute the most to snowpack ablation may simply have a higher
374 rate of occurrence and lower daily energy flux values than other types. In order to obtain a more detailed
375 understanding of each type's energy flux, mean daily energy flux calculated for each type was determined to be a
376 better method of comparison. Therefore, both mean daily (Figure 10) and total snowpack period fluxes over the



377 two seasons (Figure 11) are discussed in MJ m^{-2} to show synoptic type energy flux contributions made at short
378 and longer temporal scales.

379 3.2.1 Latent and sensible heat flux

380 Daily Q_e was negative for each of the seven synoptic types and the magnitude of the values was shown to
381 correspond to the mean 850 hPa RH values for each type, which is due to an elevation of 1828 m A.S.L. at the
382 site that resulted in an ambient pressure of 791-831 hPa for the entirety of the study period. Two of the three types
383 with the lowest RH values (T2 and T5) showed the greatest negative latent heat flux and those with the higher RH
384 values (T1 and T6) showed the least amount of latent heat flux, which is consistent with conditions needed for
385 evaporation from the snowpack. T5 had the largest negative latent heat flux of any type with a mean daily value
386 of $-1.26 \text{ MJ m}^{-2} \text{ day}^{-1}$ which corresponds to its low 850 hPa RH values, the highest observed surface mean daily
387 ambient temperature of 3.5°C , and the second lowest observed surface mean RH value of 66% with only T2 being
388 lower (61%).

389 Overall, negative Q_e was offset by positive Q_h for most types with the exception of T3 that had mean surface
390 temperatures below zero (-1.01°C) and a measured surface RH value below 90% resulting in more latent heat loss
391 than sensible heat gain by the snowpack. Similar to trends seen in the Q_e , the highest daily mean Q_h values were
392 associated with synoptic types with the highest temperatures at 850 hPa (T5, T7, & T2), which coincided with
393 observed temperatures from the energy flux tower (3.54°C , 1.42°C , & 1.04°C). T5 showed the highest daily Q_e
394 and Q_h values as a result of having the highest temperatures and lowest RH values of any type. Ultimately, when
395 both turbulent terms are considered, T5 had the highest amount of energy flux into the snowpack (1.28 MJ m^{-2}
396 day^{-1}) followed by T7 ($1.11 \text{ MJ m}^{-2} \text{ day}^{-1}$) and T2 ($0.97 \text{ MJ m}^{-2} \text{ day}^{-1}$).

397 3.2.2 Radiation flux

398 The largest contribution of radiative energy to the snowpack from all synoptic types was K^* which accounted for
399 57-81% of total positive flux. By comparison, L^* accounted for 66-90% of negative energy flux from the snowpack
400 with the highest amounts of loss belonging to the types with the lowest percentage of cloud cover (T1, T2, and
401 T3). Total radiation flux varied largely by synoptic type and was found to be positive in types T3, T6, & T5 and
402 negative for the rest of the types. The three types with positive net radiation had the highest incoming longwave
403 radiation flux values that allowed for greater cancellation of outgoing longwave values and allowed for incoming
404 shortwave radiation to dominate the net radiation flux. The largest loss in net radiation energy was exhibited by
405 T1 that was 3% higher than the next closest type (T2). The types with net radiation loss (T1, T2, T4, and T7) had
406 values that ranged from $-0.66 \text{ MJ m}^{-2} \text{ day}^{-1}$ (T4) to $-1.44 \text{ MJ m}^{-2} \text{ day}^{-1}$ (T1). However, T4 had dissimilar cloud and
407 relative humidity characteristics to T2 and T7, which had the two lowest cloud cover percentages and two of the
408 lowest RH values. T4 had 100% cloud cover and had an associated reduction in incoming shortwave radiation
409 that allowed the outgoing longwave radiation term to become more dominant than in T2 or T7 and, therefore,
410 gave it the highest net radiative energy loss of the three.

411 3.2.3 Ground and precipitation heat flux

412 Energy flux from ground and precipitation sources were the smallest of any term for all types, with ground heat
413 and precipitation fluxes accounting for less than one percent of mean daily energy fluxes for all synoptic types.
414 Ground heat flux characteristics were similar between all synoptic types and varied little. While Q_p was small



415 when examined as a daily mean value, it does show a high degree of variation that was associated with T5 and
416 T3. This is due to several large rain events that occurred during 2016 (July 18; July 21-22; and August 31) and
417 one during 2017 (August 15). Despite relatively low energy flux contributions by rainfall, it is interesting to note
418 that the ten days with the highest rainfall fluxes ($>0.05 \text{ MJ m}^{-2} \text{ day}^{-1}$) consisted of four T5 days, three T3 days,
419 two T7 days, and one T6 day showing a significant clustering of high precipitation days in types T5 and T3.

420 **3.2.4 Total daily net energy flux**

421 Overall, four synoptic types (T3, T5, T6, and T7) had positive mean daily net energy flux to the snowpack (Figure
422 12). Of these, T5 had the largest energy flux that was related to its relatively high temperatures that contributed
423 to the highest Q_h value of any synoptic type and increased solar radiation from less cloud cover. Contrary to the
424 reduction in cloud cover that aided T5 in having the highest total energy flux contributions, T6 had the highest
425 cloud cover and yet had the second highest energy flux to the snowpack that was primarily due to increased
426 incoming longwave radiation. Similarly, positive net radiation flux associated with T3 gave it a net positive daily
427 net energy flux. Positive net energy flux from T7 is a result of relatively low percentage of cloud cover and the
428 associated increase in $K \downarrow$ as well as the second highest Q_h term of any type.

429 T1 and T4 showed the greatest negative mean daily net energy flux of all synoptic types (Figure 12), which could
430 be attributed to their low Q_h values as a result of the lowest measured temperatures of any synoptic type and to
431 having low $K \downarrow$ terms. T2 also had a net negative mean daily energy flux but to a lesser extent than either T1 or
432 T4. Relative humidity values lower than any other type were the primary driver behind T2's negative net value as
433 it resulted in the highest longwave radiation loss from the snowpack through having the lowest cloud cover, as
434 well as Q_e loss.

435 T5 contributed the most energy to the snowpack during the two seasons despite T3 having nearly 96% more
436 occurrences in the same period. This was largely due to high Q_h values associated with strong WAA ahead of the
437 passage of cold fronts associated with the T5 synoptic type, which had the second largest overall energy
438 contribution to the snowpack. While mean daily energy flux contributions of T6 to snowpack energy flux are
439 103% higher than those of T3, the high number of occurrences associated with T3 made it the second highest
440 contributor of energy flux during the two seasons with T6 contributing the third highest amount of energy flux.
441 T7 had the smallest positive energy flux contribution to the snowpack during the two seasons. Types with negative
442 seasonal fluxes showed similar magnitude to their mean daily values with T1 and T4 having the first and second
443 highest negative flux, respectively, and T2 having the least negative flux.

444 All synoptic types had relatively large variation in mean daily net energy that can be attributed to the classification
445 conducted by the k-means clustering technique. Each type consisted of classified days that had similar synoptic
446 characteristics, but differences in system strength and position affected energy fluxes for individual days.
447 Therefore, it is important to remember that each synoptic type is associated with a range of daily energy flux
448 values in addition to the mean daily energy flux for each type.

449 **3.2.5 Energy balance closure**

450 Internal energy storage and melt processes can make measurement of energy balance closure over snow
451 particularly difficult when internal measurements of the snowpack aren't available (Helgason and Pomeroy,
452 2012). As measurements of snowpack properties were not available during this period, assessment of energy



453 balance closure was conducted on periods when snow surface temperatures and ambient air temperature were less
454 than 0°C to limit the amount of energy being used in internal snowpack melt processes. Energy balance data was
455 divided into day and night periods following the methods of Helgason and Pomeroy (2012) that used an incoming
456 shortwave radiation threshold of $> 200 \text{ Wm}^{-2}$ for day periods and 0 Wm^{-2} for night periods. Daytime periods
457 showed a slightly higher mean energy balance closure ratio of 0.33 ± 0.55 ($n = 761$) than night periods that had a
458 mean closure ratio of 0.31 ± 0.51 ($n = 2291$). Inability to account for nearly constant internal snowpack melt
459 processes has likely resulted in the low closure ratio and high variability in calculated energy balance closure.

460 3.3 Climatological trends of snowpack energy flux

461 3.3.1 Frequency of occurrence and trends

462 Occurrence frequencies were determined for each synoptic type by classifying each day from June-October from
463 1979 to 2017. Statistics on seasonal averages of frequency for each type are displayed in Table 6 and show that
464 T2 and T3 have the greatest number of mean seasonal occurrences with 25 and 24 days per season, respectively.
465 All other types have between 20-23 days per season with the exception of T6 that has the lowest number of
466 seasonal occurrences at 17 days. T4 and T5 had the lowest variation between seasons of ± 4 days indicating relative
467 consistency when compared to the other types that had variations of ± 5 -7 days per year.

468 Trends in occurrence frequencies of each type can be seen in Figure 13. In relation to the longer climatological
469 record, 2016 season showed a below average number of T1 days (characterised by high pressure) with only nine
470 days having the classification. In addition, it had the highest number of T3 days (characterised by pre-frontal
471 conditions) (tied with 2003) and was in the top six seasons for number of T6 events (cut-off low). The increase in
472 T3 events correspond with several rain-on-snow event days during the season that showed higher Q_r contributions
473 than would be expected based on mean daily energy flux values. 2017 had synoptic type occurrences that were
474 close to climatological means with only T4 being slightly above the occurrence standard deviation with 28 total
475 days, which is above the normal mean seasonal occurrence of 21 ± 4 days.

476 Significant variability exists between years, but linear trend analysis shows increases in frequency that can be
477 seen in T1, T2, T3, and T4 with decreases in T5, T6, and T7. T2 shows the greatest increase in frequency with a
478 gain of approximately six days annually over the 39 year period and T7 shows the largest decrease of five days
479 per season. All types associated with negative snowpack energy flux (T1, T2, and T4) have increases in their
480 seasonal frequency and T3 was the only type associated with positive snowpack energy flux that showed an
481 increase in frequency. The types associated with the largest quantities of positive snowpack energy flux (T5 and
482 T6) showed declines of 1-2 days per season.

483 Snowpack energy flux pertaining to the June-October seasons (1979-2017) was estimated using the identified
484 synoptic types and mean daily energy flux characteristics of each type identified from the 2016 and 2017
485 observational period. Similar to trends seen in the frequency of synoptic types that generally shows types
486 associated with positive (negative) snowpack energy flux decreasing (increasing), overall estimated mean
487 seasonal snowpack energy flux is shown to decrease by 7.41 MJ m^{-2} over the 39 year period (Figure 14). However,
488 estimated mean seasonal snowpack energy flux was still strongly positive for all years with only 1997 and 2013
489 having positive fluxes less than 10 MJ m^{-2} , which also showed the highest numbers of T1 and T2 that are
490 characterized as having dominant high pressure over the region.



491 **3.3.2 Atmospheric teleconnections**

492 Investigation into teleconnection impacts on estimated seasonal snowpack energy flux showed relationships with
493 IOD and SOI phase, but little relationship with SAM phase (Figure 15). A negative (positive) correlation with an
494 R^2 value of 0.47 (0.38) can be seen between IOD (SOI) phase and total seasonal snowpack energy flux, which
495 agrees with the findings of Pepler et al. (2014) who showed IOD as a greater influence on cool season precipitation
496 in SEA than ENSO. Of the ten seasons with the largest estimated positive snowpack energy flux, 7 occurred
497 during a negative IOD phase and 9 occurred during a positive SOI phase. Six of these seasons had abnormally
498 high T6 (cut-off low) counts that all fell outside of one standard deviation from the mean of 17 ± 6 days and seven
499 seasons had low T1 (high pressure). This indicates that the highest estimated snowpack energy flux seasons tend
500 to occur during a negative IOD phase and positive SOI phase through a shift from high pressure occurrences to
501 dominant cut-off lows over the region.

502 Seasons with the highest estimated positive snowpack energy flux were distributed over the climatological study
503 period with one occurring during 1979, four in the 1980s, one in the 1990s, three in the 2000s, and one in the
504 2010s. Periods of reduced energy flux are seen in the 1990s and 2010s (Figure 14), which can be attributed to
505 dominance of positive IOD phase and negative SOI phase during these periods.

506 Overall, IOD phase was the dominant climatological control of estimated seasonal energy flux and accounted for
507 an average increase of 31% when changing from a positive to negative phase (Table 7). SOI phase had a similar
508 effect accounting for a mean positive energy flux increase of 28% during seasons that were positive. While SAM
509 phase can account for an increase of 12% energy flux by season when it is negative, its contribution is relatively
510 small compared to the other two terms. Negative IOD and positive SOI can account for a 48% increase in energy
511 flux to the snowpack when compared to years with opposite phases. The highest estimated energy flux to the
512 snowpack occurs when IOD is negative, SAM is negative, and SOI is positive, which results in up to 56% more
513 energy flux to the snowpack than other periods. While the highest difference in energy flux is seen in the correct
514 combination of IOD -, SAM -, and SOI + periods when compared to others, only 40% of the top ten seasons with
515 the largest energy flux had this characteristic. However, 80% (including three of the top five seasons) had a
516 negative IOD and positive SOI suggesting that strength of phase is also an important consideration.

517 **4 Discussion**

518 **4.1 Properties of synoptic type energy balance**

519 Net shortwave radiation flux contributed the largest amount of energy to the snowpack for all synoptic types
520 ranging from 57-81% of mean daily energy flux with T5 being the only synoptic type below 60% contribution
521 (57%) of K^* to the snowpack. These results agree with Fayad et al. (2017) who noted that radiative fluxes are the
522 dominant source of snowpack melt energy in mountain ranges with Mediterranean climates. Net sensible heat flux
523 contributed the second highest percentage of mean daily energy flux to the snowpack accounting for 13-40% of
524 positive fluxes. The largest contributions of Q_h to the snowpack are associated with synoptic types T2, T5, and
525 T7 that are characterised by high pressure and northwesterly winds that are associated with WAA. Hay and
526 Fitzharris (1988) noted that, while radiative terms were responsible for the majority of energy contributions to
527 glacier melt in New Zealand's Southern Alps, turbulent fluxes contributed significant amounts of energy to melt.
528 Similarly, despite Q_h not being the dominant energy flux to the snowpack for any synoptic type, it does account



529 for nearly half of the energy flux to the snowpack for T5 (40%) and over a third for T2 (34%), and is still a
530 significant source of energy flux to the snowpack for all synoptic types.

531 Mean daily energy loss from the snowpack was from latent heat and net longwave radiation, which dominated
532 T1, T2, and T4 resulting in negative mean daily energy fluxes from the snowpack. Net longwave radiation was
533 the most influential term in the emission of energy from the snowpack accounting for 66-90% of energy loss with
534 net latent heat flux accounting for 10-27% of outgoing energy flux. Though the methodology of this paper
535 distinguishes between shortwave and longwave fluxes in order to better examine the effects of synoptic-scale
536 features such as RH or cloud cover on radiative transfers, many prior works have not made the same distinction
537 in terms (Hay and Fitzharris, 1988; Moore and Owens, 1984; Neale and Fitzharris, 1997; Stoy et al., 2018). It
538 should be noted that had Q^* been used for comparison, the results of this paper agree with several studies (Bednorz,
539 2008b; Moore and Owens, 1984; Sade et al., 2014) that found that turbulent fluxes were the dominant fluxes when
540 examining the energy flux characteristics on snowpacks in climates similar to that of the Snowy Mountains.

541 Mean daily Q_g values were found to account for only a small fraction of total energy flux to the snowpack
542 consisting of 1-4% of daily positive energy fluxes. Similarly, energy flux to the snowpack from rainfall has been
543 shown to only contribute ~1% of total seasonal energy flux for five of the seven synoptic types which agrees with
544 the findings of other studies (Bilish et al., 2018; Mazurkiewicz et al., 2008). However, precipitation was
545 responsible for ~2% of the daily mean energy flux of the two synoptic types primarily associated with rain-on-
546 snow events, T5 and T3 respectively. Although fluxes imparted on the snowpack from rainfall are relatively small
547 when compared to all positive fluxes, the accompanying energy flux characteristics of the synoptic types
548 associated with rain-on-snow events are responsible for two of the three largest contributions of overall snowpack
549 energy fluxes.

550 4.2 Synoptic patterns and energy flux

551 Snowpack energy flux characteristics recorded at the Pipers Creek catchment headwaters have been related to
552 synoptic weather types that occurred during the 2016 and 2017 snow seasons. The resulting analysis reveals a
553 maximum in positive energy flux as pre-frontal troughs approach the Snowy Mountains, followed by cold front
554 conditions during the T7→T5→T3 common progression pattern identified here. Several factors cause high
555 positive energy flux during these periods that include: an increase in temperatures due to WAA and the associated
556 increase in positive Q_h ; decrease in negative L^* due to an increase in cloud cover; a decrease in Q_e following
557 frontal passage and associated increase in RH; and progressively increasing Q_r as the trough approaches and
558 immediately after passage.

559 Synoptic types characterized by surface high pressure as their primary influence (T1, T2, T4, and T7) showed the
560 lowest contributions to snowpack energy flux. In T1, T2, and T7, net shortwave radiation terms (K^*) were positive
561 and varied by ~2-24% for these types, however, low RH and cloud cover allowed for highly negative L^* terms
562 that were not compensated by change in K^* . In contrast, T4 had higher cloud cover and increased RH that were
563 due to advection of moisture from the Tasman Sea. The higher RH in T4 and low mean air temperature (-2.06°C)
564 resulted in Q_e and Q_h terms of similar magnitudes, but opposite signs that nearly cancelled out. This resulted in a
565 L^* term that was of lesser magnitude than those of T1, T2, and T7, but still the dominant term in its energy
566 exchange.



567 Four primary synoptic circulation patterns were identified during the study period. Each of the four patterns and
568 their associated energy flux values calculated from mean daily flux and mean type duration can be seen in Figures
569 9 and 16. While each pattern differs towards the end of the cycle, each one has the T7→T5→T3 progression in
570 common. Unsurprisingly, the highest contribution of mean energy flux to the snowpack (4.95 MJ m^{-2}) is from
571 Pattern 1, which lacks the synoptic types associated with negative snowpack energy flux that the other three
572 patterns contain. Pattern 3 had the lowest contribution to snowpack energy flux (1.86 MJ m^{-2}) due to it containing
573 types with the highest net energy loss (T1 and T4), but the positive flux types (T3, T5, and T7) supplied enough
574 energy to outweigh the negative flux of T1, T2, and T4 and make the overall pattern energy flux positive.

575 **4.3 Climatological trends in estimated energy flux**

576 Estimated positive energy flux decreases over the last 39 years result from reductions in T5, T6, and T7. These
577 types accounted for a significant portion (29%) of rain and snow during the 2016-2017 study period with only T3
578 contributing more precipitation (59%). These types all share a common characteristic of an intense surface high-
579 amplitude trough or weak cut-off low. In contrast, increases are seen in T1 and T2 that are characterized by
580 negative snowpack energy flux suggesting a shift from troughs to high pressure zonal characteristics that has also
581 been noted in other parts of Australia (Hope, 2006).

582 Reductions in winter precipitation-generating synoptic types agree with other literature (Chubb et al., 2011; Fiddes
583 et al., 2015; Theobald et al., 2016) that showed a reduction in the number of days with precipitation. As T5, T6,
584 and T7 are three of the four synoptic types with positive energy flux to the snowpack, the reductions in
585 precipitation and associated reductions in energy flux available for snow melt for these types may result in a net-
586 zero change in the energy contributed to existing snowpack. This indicates a possibility that reductions in
587 snowpack depth and duration (Hennessy et al., 2008) are primarily a result of reductions in precipitation rather
588 than increases in energy fluxes to the snowpack.

589 Phases of the IOD and SOI showed significant impacts on energy flux to the snowpack through changes to the
590 frequency of synoptic types, but SAM was found to have relatively little influence similar to findings by
591 Meneghini et al. (2007). IOD was found to be the more strongly correlated with energy flux patterns which is
592 aligned with previous research (Pepler et al., 2014; Ummenhofer et al., 2009) that showed IOD as the dominant
593 control of SEA rainfall variability when compared to ENSO. Increases in energy flux to the snowpack were
594 primarily due to reductions of T1 and its associated negative energy flux and increases of T6 that has the second
595 highest positive energy flux of all synoptic types and is associated with precipitation. Despite potential increases
596 in precipitation in SEA during periods of negative IOD (Ashok et al., 2003), energy flux to the snowpack reaches
597 peak values resulting in faster melt of the snowpack that accumulates.

598 **5 Conclusions**

599 Overall, periods of pre-cold frontal passage contribute the most energy fluxes to snowpack melt due to warm air
600 advection ahead of the front, a reduction in cloud cover allowing for higher incoming shortwave radiation, and
601 the gradual development of precipitation that often contributes to rain-on-snow events. Estimated snowpack
602 energy flux in the Snowy Mountains shows a decreasing trend over the past 39 years, but reductions in snowpack
603 duration (Hennessy et al., 2008) are still seen due to reductions in cool-season precipitation (Chubb et al., 2011;
604 Theobald et al., 2016). The influence of IOD, SOI, and SAM (to a lesser extent) phase to snowpack energy flux
605 generally manifests as a shift from anti-cyclonic characteristics and lower cloud cover values seen in T1 to



606 cyclonic conditions associated with the cut-off low of T6 and 100% cloud cover. The identification and
607 understanding of these climate patterns and their impact on synoptic systems is an important step towards
608 determining snowpack energy flux and should be closely monitored as changes can indicate significant increases
609 in snowpack ablation.

610 Reductions to precipitation and snowpack energy flux can be expected to continue into the future due to impacts
611 from anthropogenic climate change on atmospheric circulation from a poleward shift of the sub-tropical jet
612 (Kushner et al., 2001) and winter-time shifts in the position and intensity of the sub-tropical ridge (Larsen and
613 Nicholls, 2009). These changes will likely result in further reduction in precipitation in the Snowy Mountains and
614 reductions in snowpack depth and duration. Australia's modelled reduction in runoff and snowmelt as a result of
615 climate change progression (Adam et al., 2009) reinforces the importance of understanding the Australian
616 snowpack and its causes of ablation.

617 While this work was conducted solely on the Australian snowpack, snowpacks in other regions such as New
618 Zealand (Hay and Fitzharris, 1988; Neale and Fitzharris, 1997), Canada (Romolo et al., 2006a; 2006b), and the
619 Arctic (Drobot and Anderson, 2001) see similar synoptic-scale effects on snowmelt to those presented here. An
620 increased burden on freshwater systems for agriculture, drinking water, and energy production will continue as
621 anthropogenic climate change and its associated effects progress (Parry et al., 2007). Therefore, continued work
622 on marginal snowpack ablation processes, such as those within the forested regions of Australia's Snowy
623 Mountains, will be important to resource management and should be explored.

624 **Data Availability**

625 All energy flux data and code used for this project (with the exception of precipitation data) can be obtained by
626 contacting Andrew Schwartz (Andrew.Schwartz@uq.edu.au). ERA-Interim reanalysis data used in this study are
627 freely available from the European Centre for Medium-Range Weather Forecasts
628 (<https://www.ecmwf.int/en/forecasts/datasets/reanalysis-datasets/era-interim>).

629 **Author Contributions**

630 AS, HM, AT, and NC designed the experiments and AS conducted them. AT developed the k-means clustering
631 and synoptic typing code. AS developed the code related to energy balance and eddy covariance measurements,
632 trends, and teleconnections. AS prepared the manuscript.

633 **Competing Interests**

634 The authors declare that they have no competing interests.

635 **Acknowledgements**

636 The authors would like to thank Shane Bilish for establishment of the Pipers Creek snowpack research catchment,
637 Michael Gray for installation and maintenance of the energy balance tower, and the Weather and Water team at
638 Snowy Hydro Limited for their contributions of data and field support during the data collection and analysis
639 process.

640

641

642



643 **References**

- 644 Adam, J. C., Hamlet, A. F., and Lettenmaier, D. P.: Implications of global climate change for snowmelt hydrology
645 in the twenty-first century, *Hydrological Processes: An International Journal*, 23, 962-972, 2009.
- 646 Ahrens, C. D.: *Meteorology today: an introduction to weather, climate, and the environment*, Cengage Learning,
647 2012.
- 648 Allan, R. P., Shine, K. P., Slingo, A., and Pamment, J.: The dependence of clear-sky outgoing long-wave radiation
649 on surface temperature and relative humidity, *Quarterly Journal of the Royal Meteorological Society*
650 125, 2103-2126, 1999.
- 651 Ashok, K., Guan, Z., and Yamagata, T.: Influence of the Indian Ocean Dipole on the Australian winter rainfall,
652 30, doi:10.1029/2003GL017926, 2003.
- 653 Bednorz, E.: Synoptic conditions of snow occurrence in Budapest, *Meteorologische Zeitschrift*, 17, 39-45,
654 10.1127/0941-2948/2008/0262, 2008a.
- 655 Bednorz, E.: Synoptic reasons for heavy snowfalls in the Polish–German lowlands, 92, 133-140, 2008b.
- 656 Bednorz, E.: Synoptic conditions of the occurrence of snow cover in central European lowlands, 31, 1108-1118,
657 2011.
- 658 Beniston, M.: Climatic Change in Mountain Regions: A Review of Possible Impacts, *Climatic Change*, 59, 5-31,
659 10.1023/a:1024458411589, 2003.
- 660 Bilish, S. P., McGowan, H. A., and Callow, J. N.: Energy balance and snowmelt drivers of a marginal subalpine
661 snowpack, *Hydrol Process*, 32, 3837-3851, 2018.
- 662 Budin, G.: Interannual variability of Australian snowfall, *Aust. Met. Mag*, 33, 145-159, 1985.
- 663 BOM: Analysis Chart Archive: <http://www.bom.gov.au/australia/charts/archive/>, access: 15.09.2018, 2018.
- 664 Cai, W., Shi, G., Cowan, T., Bi, D., and Ribbe, J.: The response of the Southern Annular Mode, the East Australian
665 Current, and the southern mid-latitude ocean circulation to global warming, 32, doi:10.1029/2005GL024701,
666 2005.
- 667 Cai, W., Cowan, T., and Raupach, M.: Positive Indian Ocean Dipole events precondition southeast Australia
668 bushfires, *Geophys Res Lett*, 36, 10.1029/2009GL039902, 2009a.
- 669 Cai, W., Cowan, T., and Sullivan, A.: Recent unprecedented skewness towards positive Indian Ocean Dipole
670 occurrences and its impact on Australian rainfall, *Geophys Res Lett*, 36, 10.1029/2009GL037604, 2009b.



- 671 Callow, N., McGowan, H., Warren, L., and Speirs, J.: Drivers of precipitation stable oxygen isotope variability in
672 an alpine setting, Snowy Mountains, Australia, *Journal of Geophysical Research: Atmospheres*, 119, 3016-3031,
673 10.1002/2013JD020710, 2014.
- 674 Campbell Scientific EC150 CO₂/H₂O Open-Path Gas Analyzer: <https://www.campbellsci.com/manuals>, access:
675 24.10.2018, 2018a.
- 676 Campbell Scientific EasyFlux DL CR3000OP: <https://www.campbellsci.com/manuals>, access: 15.2.2018, 2018b.
- 677 Chubb, T. H., Siems, S. T., and Manton, M. J.: On the Decline of Wintertime Precipitation in the Snowy
678 Mountains of Southeastern Australia, *J Hydrometeorol*, 12, 1483-1497, 10.1175/Jhm-D-10-05021.1, 2011.
- 679 Costin, A. B., and Gay, D.: *Studies in Catchment Hydrology in the Australian Alps*, MPKV; Maharashtra, 1961.
- 680 Dee, D. P., Uppala, S. M., Simmons, A., Berrisford, P., Poli, P., Kobayashi, S., Andrae, U., Balmaseda, M.,
681 Balsamo, G., and Bauer, d. P.: The ERA-Interim reanalysis: Configuration and performance of the data
682 assimilation system, *Quarterly Journal of the royal meteorological society*, 137, 553-597, 2011.
- 683 Drobot, S. D., and Anderson, M. R.: Comparison of interannual snowmelt-onset dates with atmospheric
684 conditions, *Annals of Glaciology*, 33, 79-84, 2001.
- 685 Duus, A. L.: Estimation and analysis of snow cover in the Snowy Mountains between 1910 and 1991, *Aust*
686 *Meteorol Mag*, 40, 195-204, 1992.
- 687 Falge, E., Baldocchi, D., Olson, R., Anthoni, P., Aubinet, M., Bernhofer, C., Burba, G., Ceulemans, G., Clement,
688 R., Dolman, H., Granier, A., Gross, P., Grunwald, T., Hollinger, D., Jensen, N. O., Katul, G., Keronen, P.,
689 Kowalski, A., Lai, C. T., Law, B. E., Meyers, T., Moncrieff, J., Moors, E., Munger, J. W., Pilegaard, K., Rannik,
690 U., Rebmann, C., Suyker, A., Tenhunen, J., Tu, K., Verma, S., Vesala, T., Wilson, K., and Wofsy, S.: Gap filling
691 strategies for long term energy flux data sets, *Agr Forest Meteorol*, 107, 71-77, Doi 10.1016/S0168-
692 1923(00)00235-5, 2001a.
- 693 Falge, E., Baldocchi, D., Olson, R., Anthoni, P., Aubinet, M., Bernhofer, C., Burba, G., Ceulemans, R., Clement,
694 R., Dolman, H., Granier, A., Gross, P., Grunwald, T., Hollinger, D., Jensen, N. O., Katul, G., Keronen, P.,
695 Kowalski, A., Lai, C. T., Law, B. E., Meyers, T., Moncrieff, H., Moors, E., Munger, J. W., Pilegaard, K., Rannik,
696 U., Rebmann, C., Suyker, A., Tenhunen, J., Tu, K., Verma, S., Vesala, T., Wilson, K., and Wofsy, S.: Gap filling
697 strategies for defensible annual sums of net ecosystem exchange, *Agr Forest Meteorol*, 107, 43-69, Doi
698 10.1016/S0168-1923(00)00225-2, 2001b.
- 699 Fayad, A., Gascoin, S., Faour, G., López-Moreno, J. I., Drapeau, L., Le Page, M., and Escadafal, R.: Snow
700 hydrology in Mediterranean mountain regions: A review, *J Hydrol*, 551, 374-396, 2017.
- 701 Fiddes, S. L., Pezza, A. B., and Barras, V.: A new perspective on Australian snow, *Atmospheric Science Letters*,
702 16, 246-252, 10.1002/asl2.549, 2015.



- 703 Foken, T., Leuning, R., Oncley, S. R., Mauder, M., and Aubinet, M.: Corrections and data quality control, in:
704 Eddy covariance, Springer, 85-131, 2012.
- 705 Gellie, N. J. H.: Native vegetation of the Southern Forests: South-east highlands, Australian alps, south-west
706 slopes and SE corner bioregions, Royal Botanic Gardens, 2005.
- 707 Goree, P. A., and Younkin, R. J.: Synoptic Climatology of Heavy Snowfall Over the Central and Eastern United
708 States, 94, 663-668, 10.1175/1520-0493(1966)094<0663:Scosho>2.3.Co;2, 1966.
- 709 Gray, M. A., McGowan, H. A., Lowry, A. L., and Guyot, A.: Surface energy exchanges over contrasting
710 vegetation types on a sub-tropical sand island, Agr Forest Meteorol, 249, 81-99, 10.1016/j.agrformet.2017.11.018,
711 2018.
- 712 Grundstein, A. J., and Leathers, D. J.: A case study of the synoptic patterns influencing midwinter snowmelt
713 across the northern Great Plains, 12, 2293-2305, doi:10.1002/(SICI)1099-1085(199812)12:15<2293::AID-
714 HYP797>3.0.CO;2-9, 1998.
- 715 Hay, J. E., and Fitzharris, B. B.: The synoptic climatology of ablation on a New Zealand glacier, Journal of
716 Climatology, 8, 201-215, 10.1002/joc.3370080207, 1988.
- 717 Helgason, W., and Pomeroy, J.: Problems Closing the Energy Balance over a Homogeneous Snow Cover during
718 Midwinter, J Hydrometeorol, 13, 557-572, 10.1175/Jhm-D-11-0135.1, 2012.
- 719 Hendon, H. H., Thompson, D. W. J., and Wheeler, M. C.: Australian Rainfall and Surface Temperature Variations
720 Associated with the Southern Hemisphere Annular Mode, 20, 2452-2467, 10.1175/jcli4134.1, 2007.
- 721 Hennessy, K. J., Whetton, P. H., Walsh, K., Smith, I. N., Bathols, J. M., Hutchinson, M., and Sharples, J.: Climate
722 change effects on snow conditions in mainland Australia and adaptation at ski resorts through snowmaking, Clim
723 Res, 35, 255-270, 10.3354/cr00706, 2008.
- 724 Hope, P. K.: Projected future changes in synoptic systems influencing southwest Western Australia, J Climate
725 Dynamics, 26, 765-780, 10.1007/s00382-006-0116-x, 2006.
- 726 Hope, P. K., Drosowsky, W., and Nicholls, N. J. C. D.: Shifts in the synoptic systems influencing southwest
727 Western Australia, 26, 751-764, 10.1007/s00382-006-0115-y, 2006.
- 728 Kidson, J. W.: An analysis of New Zealand synoptic types and their use in defining weather regimes, International
729 journal of climatology, 20, 299-316, 2000.
- 730 Kushner, P. J., Held, I. M., and Delworth, T. L.: Southern Hemisphere Atmospheric Circulation Response to
731 Global Warming, 14, 2238-2249, 10.1175/1520-0442(2001)014<0001:Shact>2.0.Co;2, 2001.
- 732 Larsen, S. H., and Nicholls, N.: Southern Australian rainfall and the subtropical ridge: Variations,
733 interrelationships, and trends, 36, doi:10.1029/2009GL037786, 2009.



- 734 Male, D. H., and Granger, R. J.: Snow Surface-Energy Exchange, *Water Resour Res*, 17, 609-627, DOI
735 10.1029/WR017i003p00609, 1981.
- 736 Mazurkiewicz, A. B., Callery, D. G., and McDonnell, J. J.: Assessing the controls of the snow energy balance and
737 water available for runoff in a rain-on-snow environment, *J Hydrol*, 354, 1-14, 2008.
- 738 McKay, D. C., and Thurtell, G. W.: Measurements of the energy fluxes involved in the energy budget of a snow
739 cover, *J Appl Meteorol*, 17, 339-349, 1978.
- 740 Meneghini, B., Simmonds, I., and Smith, I. N.: Association between Australian rainfall and the Southern Annular
741 Mode, *International Journal of Climatology*, 27, 109-121, 10.1002/joc.1370, 2007.
- 742 Michelson, D. B.: Systematic correction of precipitation gauge observations using analyzed meteorological
743 variables, *J Hydrol*, 290, 161-177, 2004.
- 744 Moore, R., and Owens, I.: Controls on advective snowmelt in a maritime alpine basin, *Journal of Climate and
745 Applied Meteorology*
- 746 23, 135-142, 1984.
- 747 Neale, S. M., and Fitzharris, B. B.: Energy balance and synoptic climatology of a melting snowpack in the
748 Southern Alps, New Zealand, *International Journal of Climatology*, 17, 1595-1609, 10.1002/(SICI)1097-
749 0088(19971130)17:14<1595::AID-JOC213>3.0.CO;2-7, 1997.
- 750 Nicholls, N.: Climate variability, climate change and the Australian snow season, *Aust Meteorol Mag*, 54, 177-
751 185, 2005.
- 752 Pachauri, R. K., Allen, M. R., Barros, V. R., Broome, J., Cramer, W., Christ, R., Church, J. A., Clarke, L., Dahe,
753 Q., and Dasgupta, P.: Climate change 2014: synthesis report. Contribution of Working Groups I, II and III to the
754 fifth assessment report of the Intergovernmental Panel on Climate Change, IPCC, 2014.
- 755 Parry, M., Parry, M. L., Canziani, O., Palutikof, J., Van der Linden, P., and Hanson, C.: Climate change 2007-
756 impacts, adaptation and vulnerability: Working group II contribution to the fourth assessment report of the IPCC,
757 Cambridge University Press, 2007.
- 758 Pepler, A., Timbal, B., Rakich, C., and Coutts-Smith, A.: Indian Ocean Dipole Overrides ENSO's Influence on
759 Cool Season Rainfall across the Eastern Seaboard of Australia, 27, 3816-3826, 10.1175/jcli-d-13-00554.1, 2014.
- 760 Pook, M. J., McIntosh, P. C., and Meyers, G. A.: The synoptic decomposition of cool-season rainfall in the
761 southeastern Australian cropping region, *Journal of Applied Meteorology Climatology*, 45, 1156-1170, 2006.
- 762 Pook, M. J., Risbey, J., and McIntosh, P.: East coast lows, atmospheric blocking and rainfall: a Tasmanian
763 perspective, *IOP Conference Series: Earth and Environmental Science*, 2010, 012011,



- 764 Pook, M. J., Risbey, J. S., and McIntosh, P. C.: The synoptic climatology of cool-season rainfall in the central
765 wheatbelt of Western Australia, *Monthly Weather Review*, 140, 28-43, 2012.
- 766 Pook, M. J., Risbey, J. S., and McIntosh, P. C.: A comparative synoptic climatology of cool-season rainfall in
767 major grain-growing regions of southern Australia, *Theoretical Applied Climatology*, 117, 521-533,
768 10.1007/s00704-013-1021-y, 2014.
- 769 Prezerakos, N. G., and Angouridakis, V. E.: Synoptic consideration of snowfall in Athens, *Journal of Climatology*,
770 4, 269-285, 10.1002/joc.3370040305, 1984.
- 771 Rasmussen, R., Baker, B., Kochendorfer, J., Meyers, T., Landolt, S., Fischer, A. P., Black, J., Theriault, J. M.,
772 Kucera, P., Gochis, D., Smith, C., Nitu, R., Hall, M., Ikeda, K., and Gutmann, E.: How Well Are We Measuring
773 Snow? The NOAA/FAA/NCAR Winter Precipitation Test Bed, *B Am Meteorol Soc*, 93, 811-829, 10.1175/Bams-
774 D-11-00052.1, 2012.
- 775 Reba, M. L., Link, T. E., Marks, D., and Pomeroy, J.: An assessment of corrections for eddy covariance measured
776 turbulent fluxes over snow in mountain environments, *Water Resour Res*, 45, Artn W00d38
777 10.1029/2008wr007045, 2009.
- 778 Reinfelds, I., Swanson, E., Cohen, T., Larsen, J., and Nolan, A.: Hydrospatial assessment of streamflow yields
779 and effects of climate change: Snowy Mountains, Australia, *J Hydrol*, 512, 206-220,
780 10.1016/j.jhydrol.2014.02.038, 2014.
- 781 Robock, A.: The seasonal cycle of snow cover, sea ice and surface albedo, *Monthly Weather Review*, 108, 267-
782 285, 1980.
- 783 Romolo, L., Prowse, T. D., Blair, D., Bonsal, B. R., Marsh, P., and Martz, L. W.: The synoptic climate controls
784 on hydrology in the upper reaches of the Peace River Basin. Part II: Snow ablation, 20, 4113-4129,
785 doi:10.1002/hyp.6422, 2006a.
- 786 Romolo, L., Prowse, T. D., Blair, D., Bonsal, B. R., and Martz, L. W.: The synoptic climate controls on hydrology
787 in the upper reaches of the Peace River Basin. Part I: snow accumulation, 20, 4097-4111, doi:10.1002/hyp.6421,
788 2006b.
- 789 Ruckstuhl, C., Philipona, R., Morland, J., and Ohmura, A.: Observed relationship between surface specific
790 humidity, integrated water vapor, and longwave downward radiation at different altitudes, *Journal of Geophysical*
791 *Research: Atmospheres*, 112, 2007.
- 792 Sade, R., Rimmer, A., Litaor, M. I., Shamir, E., and Furman, A.: Snow surface energy and mass balance in a warm
793 temperate climate mountain, *J Hydrol*, 519, 848-862, 2014.
- 794 Snowy Hydro Limited Snow Depths Calculator: [https://www.snowyhydro.com.au/our-](https://www.snowyhydro.com.au/our-energy/water/inflows/snow-depths-calculator/)
795 [energy/water/inflows/snow-depths-calculator/](https://www.snowyhydro.com.au/our-energy/water/inflows/snow-depths-calculator/), access: 03/08/2018, 2018.



- 796 Stone, R., and Auliciems, A.: SOI phase relationships with rainfall in eastern Australia, *International Journal of*
797 *Climatology*, 12, 625-636, 10.1002/joc.3370120608, 1992.
- 798 Stoy, P. C., Peitzsch, E., Wood, D., Rottinghaus, D., Wohlfahrt, G., Goulden, M., and Ward, H.: On the exchange
799 of sensible and latent heat between the atmosphere and melting snow, *Agricultural Forest Meteorology*, 252, 167-
800 174, 2018.
- 801 Stull, R.: Wet-Bulb Temperature from Relative Humidity and Air Temperature, *J Appl Meteorol Clim*, 50, 2267-
802 2269, 10.1175/Jamc-D-11-0143.1, 2011.
- 803 Sturm, M., Holmgren, J., and Liston, G. E.: A seasonal snow cover classification system for local to global
804 applications, *J Climate*, 8, 1261-1283, 1995.
- 805 Theobald, A., McGowan, H., Speirs, J., and Callow, N.: A Synoptic Classification of Inflow-Generating
806 Precipitation in the Snowy Mountains, Australia, *J Appl Meteorol Clim*, 54, 1713-1732, 10.1175/Jamc-D-14-
807 0278.1, 2015.
- 808 Theobald, A., McGowan, H., and Speirs, J.: Trends in synoptic circulation and precipitation in the Snowy
809 Mountains region, Australia, in the period 1958-2012, *Atmos Res*, 169, 434-448, 10.1016/j.atmosres.2015.05.007,
810 2016.
- 811 Ueno, K.: Synoptic conditions causing nonmonsoon snowfalls in the Tibetan Plateau, *Geophys Res Lett*, 32, 2005.
- 812 Ummenhofer, C. C., England, M. H., McIntosh, P. C., Meyers, G. A., Pook, M. J., Risbey, J. S., Gupta, A. S., and
813 Taschetto, A. S.: What causes southeast Australia's worst droughts?, *Geophys Res Lett*, 36,
814 10.1029/2008GL036801, 2009.
- 815 Viviroli, D., Durr, H. H., Messerli, B., Meybeck, M., and Weingartner, R.: Mountains of the world, water towers
816 for humanity: Typology, mapping, and global significance, *Water Resour Res*, 43, Artn W07447
817 10.1029/2006wr005653, 2007.
- 818 Webb, E. K., Pearman, G. I., and Leuning, R.: Correction of flux measurements for density effects due to heat
819 and water vapour transfer, *Quarterly Journal of the Royal Meteorological Society*, 106, 85-100, 1980.
- 820 Webb, M., Slingol, A., and Stephens, G.: Seasonal variations of the clear-sky greenhouse effect: The role of
821 changes in atmospheric temperatures and humidities, *Climate dynamics*, 9, 117-129, 1993.
- 822 Whetton, P. H., Haylock, M. R., and Galloway, R.: Climate change and snow-cover duration in the Australian
823 Alps, *Climatic Change*, 32, 447-479, Doi 10.1007/Bf00140356, 1996.
- 824 Wilczak, J. M., Oncley, S. P., and Stage, S. A.: Sonic anemometer tilt correction algorithms, *Bound-Lay Meteorol*,
825 99, 127-150, Doi 10.1023/A:1018966204465, 2001.
- 826 Wilks, D. S.: Cluster analysis, in: *International geophysics*, Elsevier, 603-616, 2011.



827 Worboys, G. L., and Good, R. B.: Caring For Our Australian Alps Catchments: Summary Report For Policy
828 Makers, 2011.

829

830

831

832

833

834

835

836

837

838

839

840

841

842

843

844

845

846

847

848

849

850

851

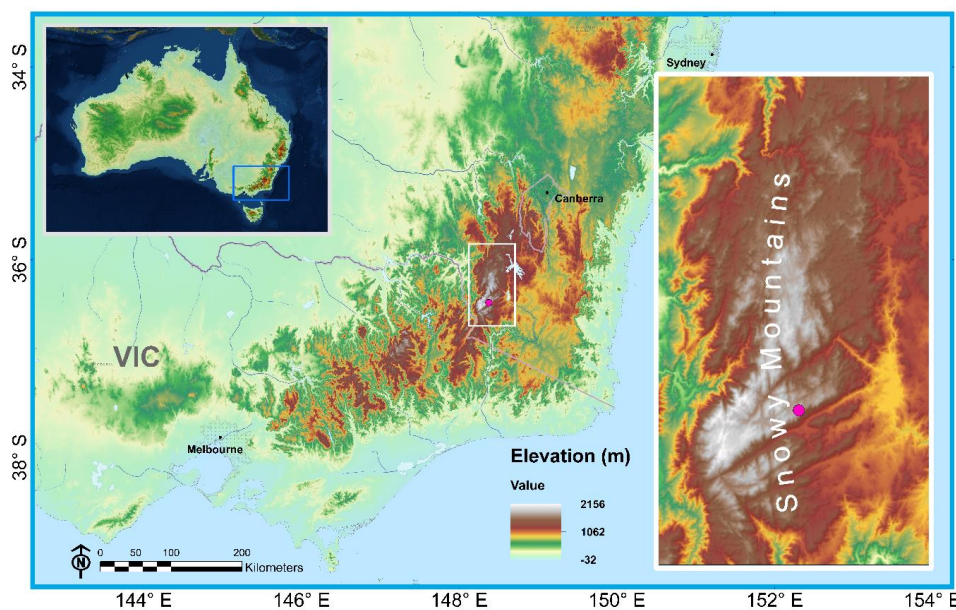
852

853

854



855
856
857
858
859
860
861
862

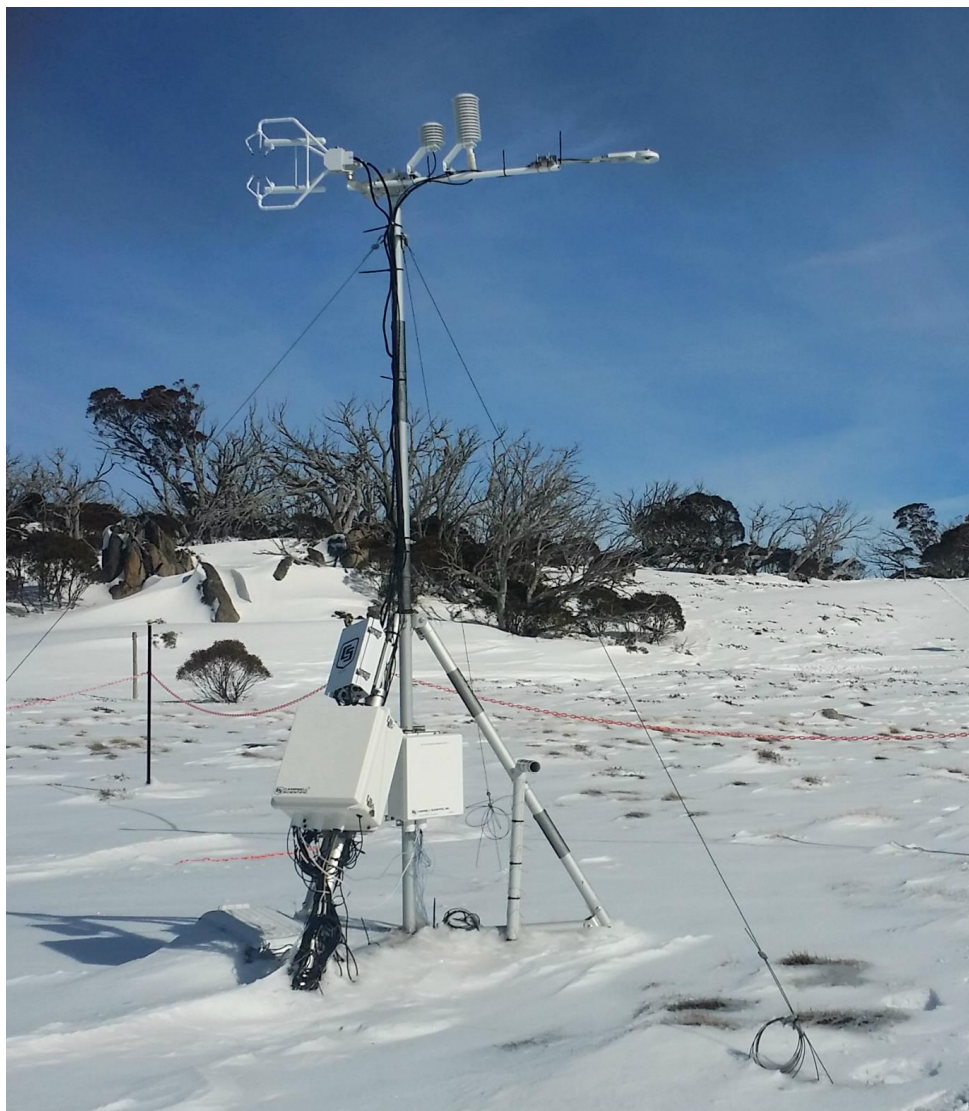


863 **Figure 1: Map of southeast Australia and the Snowy Mountains. Pink dot represents the location of the energy balance**
864 **instrumentation site.**

865
866
867
868
869
870



871
872
873
874

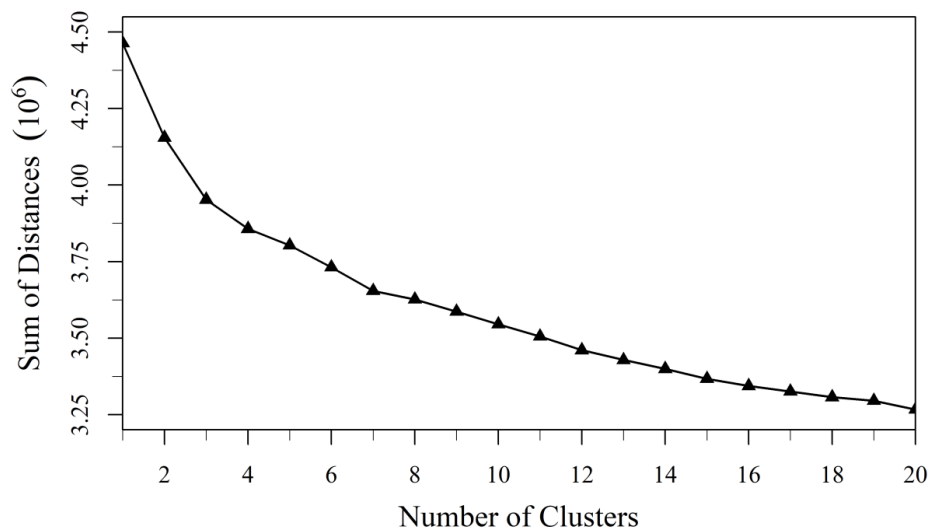


875 **Figure 2: Energy balance field site with eddy covariance instrumentation at Pipers Creek catchment headwaters.**

876
877



878
879
880
881
882
883
884
885

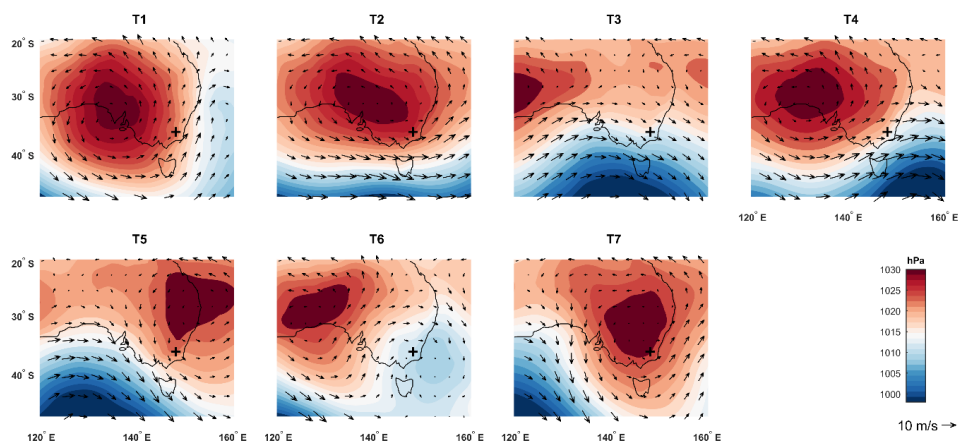


886 **Figure 3: Plot of cluster distances from centroid with a clear elbow at 7 clusters illustrating the optimum number to be**
887 **used in analysis.**

888
889
890
891
892
893



894
895
896
897
898
899
900
901
902
903

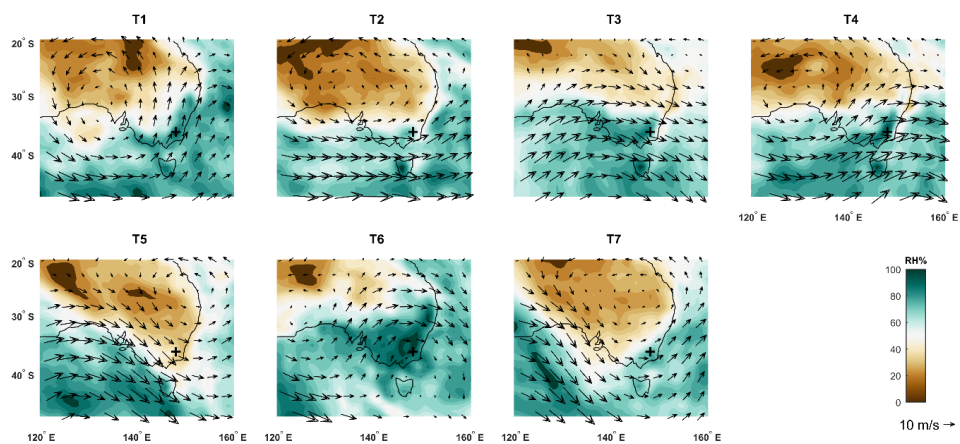


904 **Figure 4: Mean MSLP and 10m wind vectors for each synoptic type over the southeast Australia region for the 2016**
905 **and 2017 seasons. Location of surface energy balance site marked with '+'.**

906
907
908
909
910
911
912
913



914
915
916
917
918
919
920
921
922
923

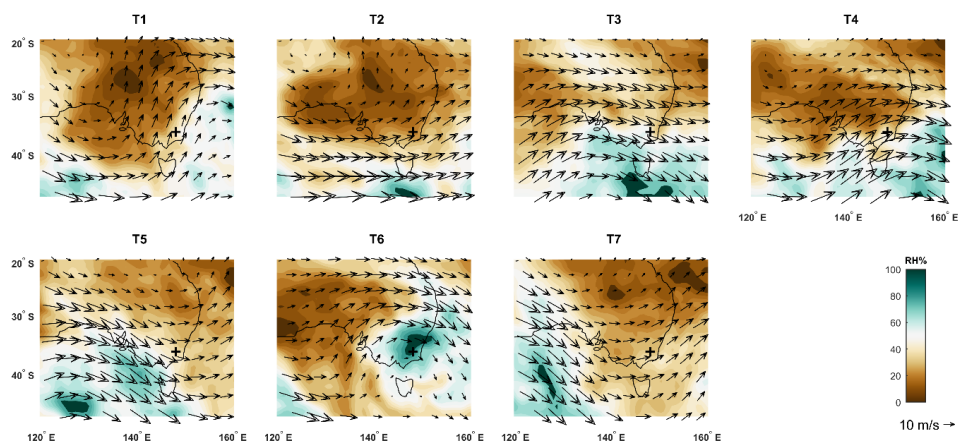


924 **Figure 5: Mean 850 hPa relative humidity values and wind vectors for each synoptic type over the southeast Australia**
925 **region for the 2016 and 2017 seasons. Location of surface energy balance site marked with '+.**

926
927
928
929
930
931
932
933



934
935
936
937
938
939
940
941
942
943

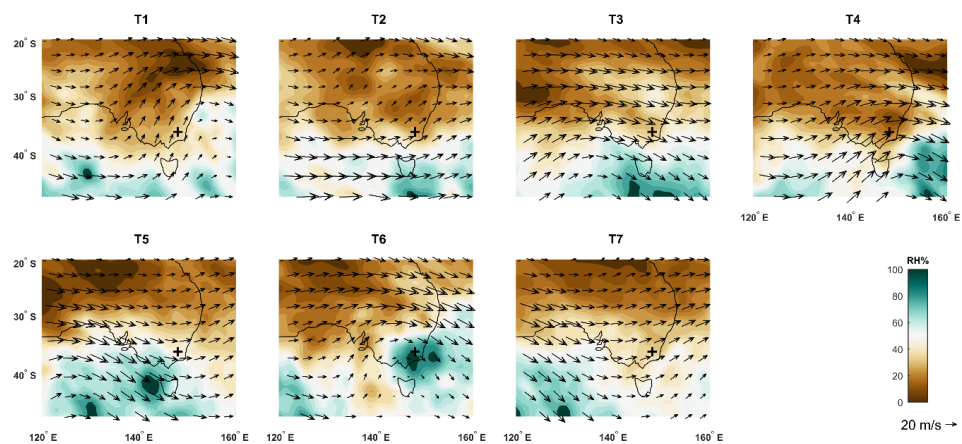


944 **Figure 6: Mean 700 hPa relative humidity values and wind vectors for each synoptic type over the southeast Australia**
945 **region for the 2016 and 2017 seasons. Location of surface energy balance site marked with '+.**

946
947
948
949
950
951
952
953



954
955
956
957
958
959
960
961
962
963

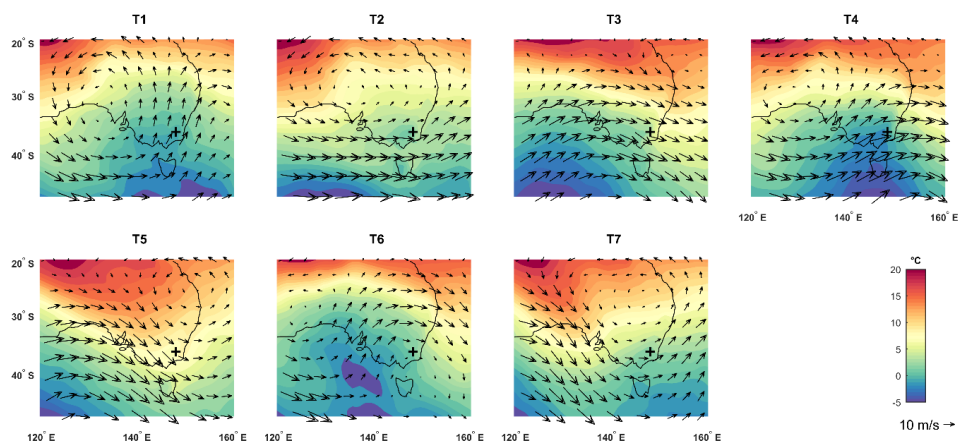


964 **Figure 7: Mean 500 hPa relative humidity values and wind vectors for each synoptic type over the southeast Australia**
965 **region for the 2016 and 2017 seasons. Location of surface energy balance site marked with '+.**

966
967
968
969
970
971
972
973



974
975
976
977
978
979
980
981
982
983



984 **Figure 8: Mean 850hPa temperature values and wind vectors for each synoptic type over the southeast Australia region**
985 **for the 2016 and 2017 seasons. Location of surface energy balance site marked with '+'.**

986
987
988
989
990
991
992
993



994

995

996

997

998

999

1000

1001

1002

1003

1004

1005

1006

1007

1008

1009

1010

1011

1012

1013

1014

1015

1016

1017

1018

1019

1020

1021

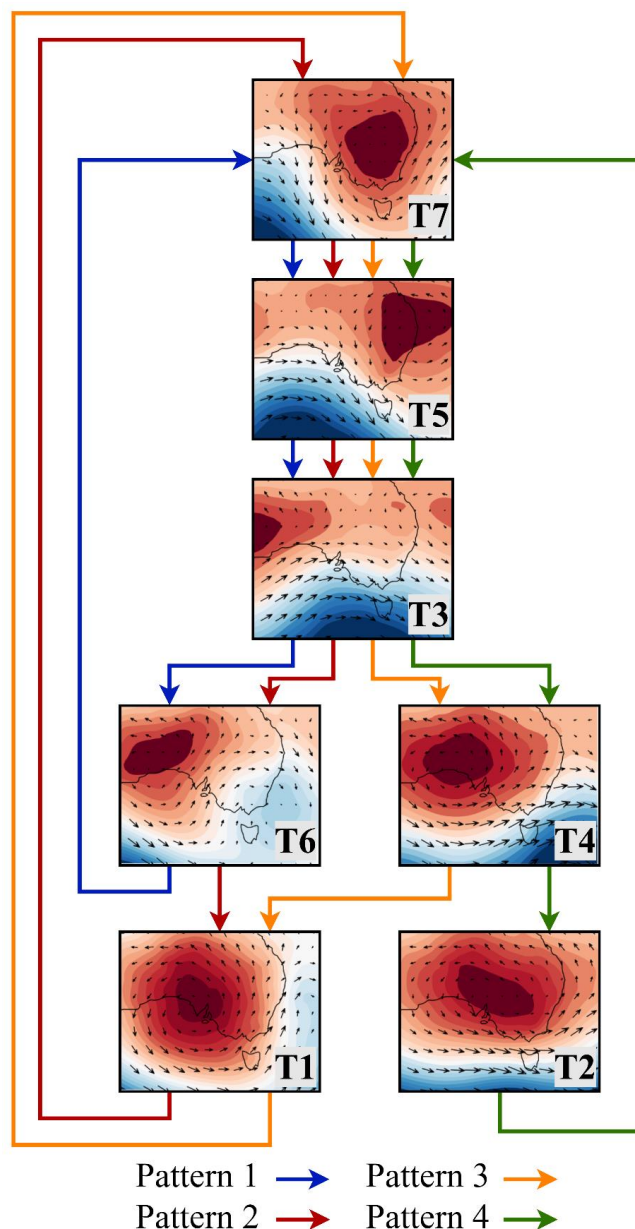
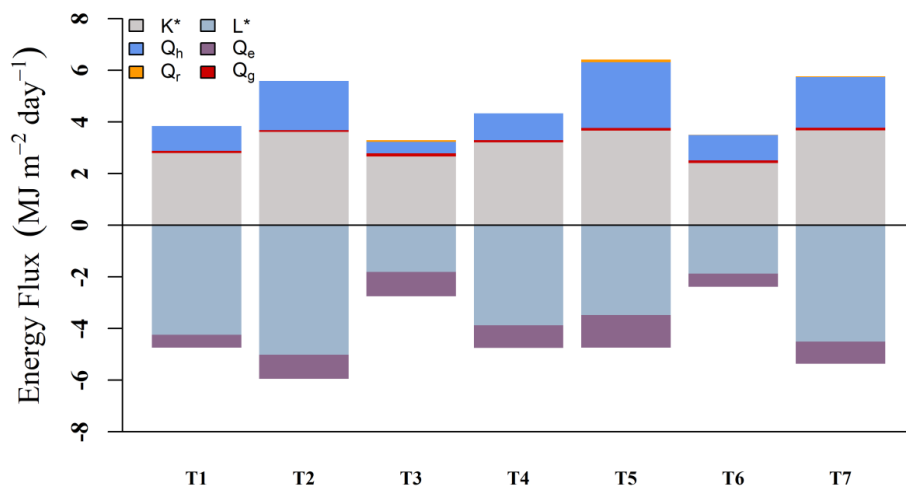


Figure 9: Flowchart of four primary synoptic type patterns/progressions based on probability of transition for the 2016 and 2017 seasons.



1022
1023
1024
1025
1026
1027
1028
1029

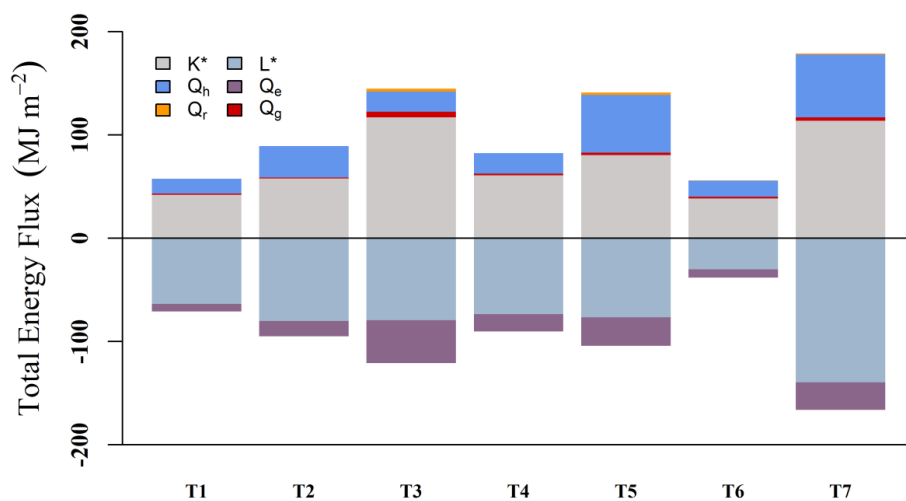


1030 Figure 10: Mean daily snowpack energy fluxes by term for each synoptic type for the 2016 and 2017 seasons.

1031
1032
1033
1034
1035
1036



1037
 1038
 1039
 1040
 1041
 1042
 1043
 1044

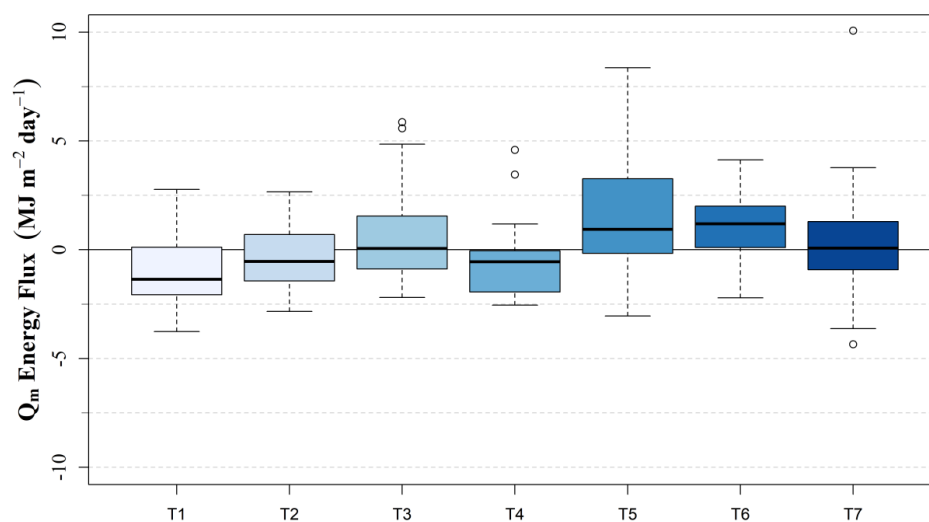


1045 **Figure 11: Total snowpack energy fluxes by term for each synoptic type during study period for the 2016 and 2017**
 1046 **seasons.**

1047
 1048
 1049
 1050
 1051
 1052



1053
1054
1055
1056
1057
1058
1059
1060



1061 **Figure 12: Box and whisker plot of daily snowpack energy fluxes by synoptic type for the 2016 and 2017 seasons.**

1062
1063
1064
1065
1066
1067
1068



1069

1070

1071

1072

1073

1074

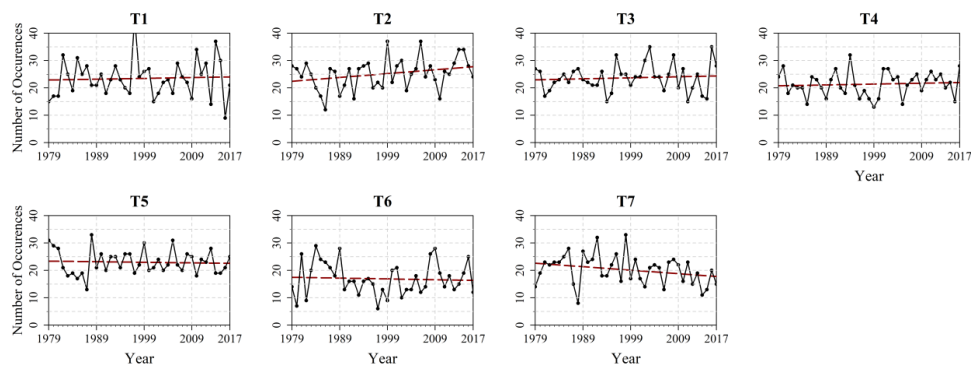
1075

1076

1077

1078

1079



1080 **Figure 13: Climatological trends in the seasonal frequency of each synoptic type from 1979 to 2017 indicated by the**
1081 **red dashed line.**

1082

1083

1084

1085

1086

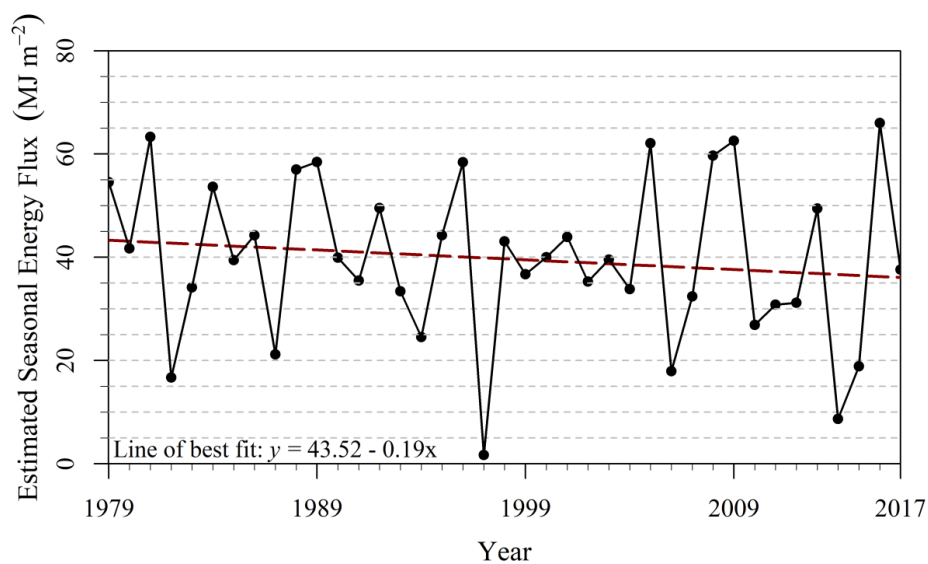
1087

1088

1089



1090
1091
1092
1093
1094
1095
1096
1097



1098 **Figure 14: Trend in estimated seasonal snowpack energy flux.**

1099
1100
1101
1102
1103
1104



1105

1106

1107

1108

1109

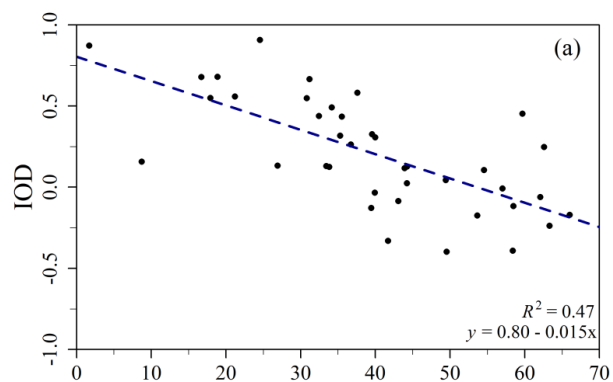
1110

1111

1112

1113

1114



1115

1116

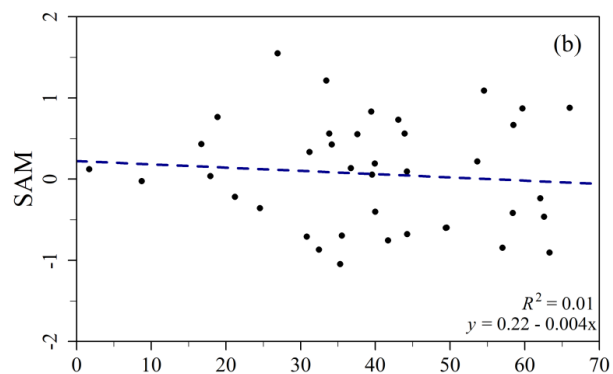
1117

1118

1119

1120

1121



1122

1123

1124

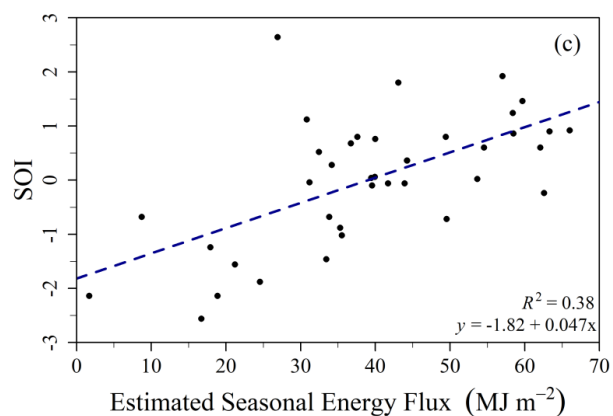
1125

1126

1127

1128

1129



1130

1131 **Figure 15: Correlation between Seasonal Snowpack Energy Flux and Indian Ocean Dipole (IOD) phase (a), Southern**

1132 **Annular Mode (SAM) phase (b), and Southern Oscillation Index (SOI) phase (c).**



1133

1134

1135

1136

1137

1138

1139

1140

1141

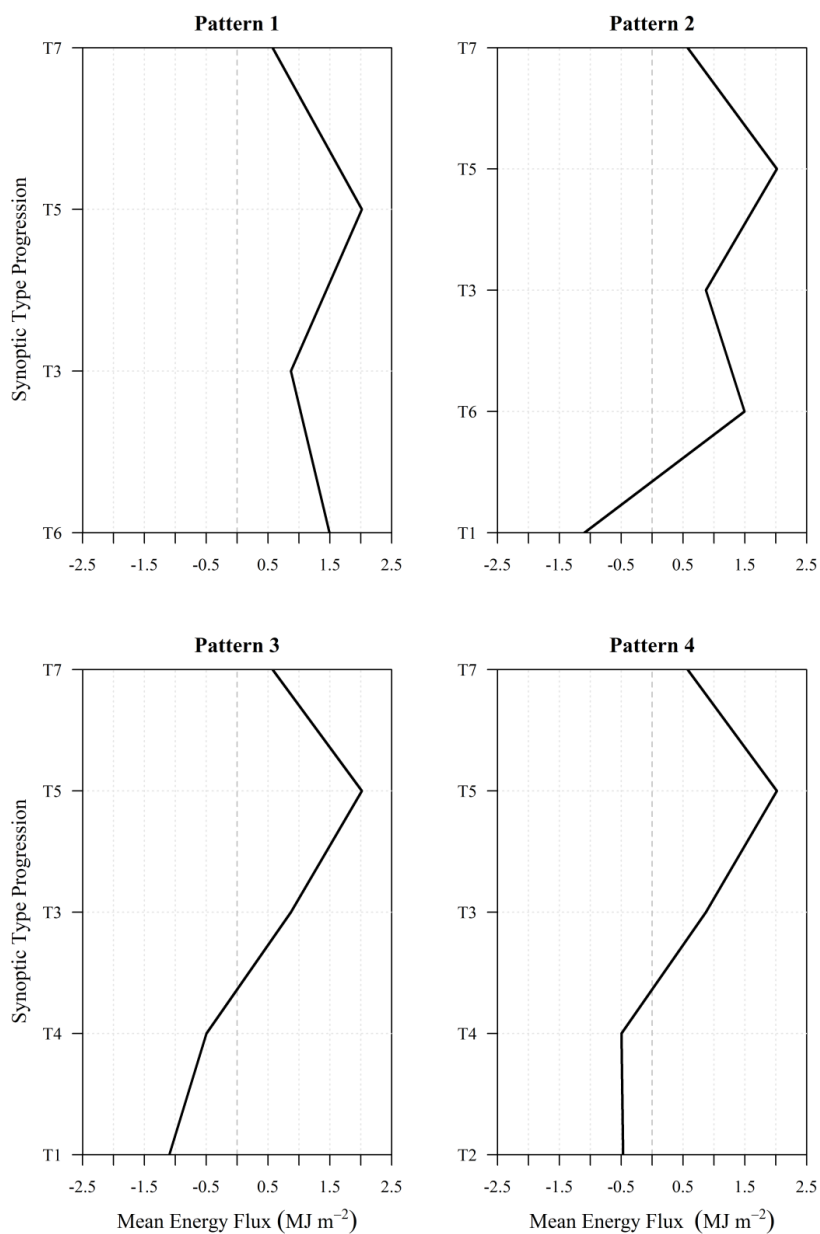
1142

1143

1144

1145

1146



1147

1148

1149

1150

1151

1152

1153

1154

1155

1156

1157

1158

1159 **Figure 16: Calculated synoptic pattern snowpack fluxes based on mean daily values and mean duration of synoptic**
1160 **type.**



1161

Instrument	Manufacturer	Variables Measured	Accuracy
SI-111	Apogee Instruments	Surface Temperature (T_{sfc})	$\pm 0.2^{\circ}\text{C}$ $-10^{\circ}\text{C} < T < 65^{\circ}\text{C}$ $\pm 0.5^{\circ}\text{C}$ $-40^{\circ}\text{C} < T < 70^{\circ}\text{C}$
CS650	Campbell Scientific	Soil Water Content (SWC)	$\pm 3\%$ SWC
		Soil Temperature	$\pm 5^{\circ}\text{C}$
CSAT3A	Campbell Scientific	Wind Components (u_x , u_y , u_z); Wind Speed (u) and Direction ($^{\circ}$); and Sonic Temperature	$\pm 5 \text{ cm s}^{-1}$
EC150	Campbell Scientific	H ₂ O Gas Density	2%
NOAH II	ETI Instrument Systems	Precipitation Accumulation	$\pm 0.254 \text{ mm}$
HFP01	Hukseflux	Soil Heat Flux	$< 3\%$
CNR4	Kipp and Zonen	K_{\downarrow} , K_{\uparrow} , L_{\downarrow} , L_{\uparrow}	$K < 5\%$ Daily Total $L < 10\%$ Daily Total
HMP155	Vaisala	Air Temperature (T_d)	$< 0.3^{\circ}\text{C}$
		Relative Humidity (RH)	$< 1.8\%$ RH
PTB110	Vaisala	Barometric Pressure	$\pm 0.15 \text{ kPa}$

1162

1163 **Table 1: Information on instruments used at the Pipers Creek catchment site.**

1164

1165

1166

1167

1168

1169

1170

1171

1172

1173

1174

1175

1176



1177

Synoptic Type	T1	T2	T3	T4	T5	T6	T7
Surface Characteristics	High pressure; SW winds	High pressure; WNW winds	Frontal; NW winds	High/low transition; W winds	High Pressure; NNW winds	Lee-side low; SW winds	High pressure; WNW winds
Cloud Cover (% days with any cover)	87.50%	76.47%	89.13%	100.00%	87.50%	100.00%	76.47%
Q_h (MJ m ⁻² day ⁻¹)	0.96	1.91	0.44	1.04	2.54	0.98	1.97
Q_e (MJ m ⁻² day ⁻¹)	-0.49	-0.94	-0.94	-0.88	-1.26	-0.51	-0.86
K_{\downarrow} (MJ m ⁻² day ⁻¹)	12.57	15.17	9.39	13.47	12.94	9.33	12.93
K_{\uparrow} (MJ m ⁻² day ⁻¹)	-9.77	-11.55	-6.72	-10.26	-9.28	-6.91	-9.25
L_{\downarrow} (MJ m ⁻² day ⁻¹)	20.08	20.14	24.78	21.89	23.66	24.66	21.80
L_{\uparrow} (MJ m ⁻² day ⁻¹)	-24.32	-25.15	-26.59	-25.76	-27.14	-26.53	-26.31
Q_g (MJ m ⁻² day ⁻¹)	0.08	0.06	0.13	0.09	0.11	0.10	0.10
Q_r (MJ m ⁻² day ⁻¹)	0.00	0.00	0.06	0.00	0.10	0.01	0.02
Q_m (MJ m ⁻² day ⁻¹)	-0.89	-0.36	0.55	-0.42	1.68	1.12	0.40
Q_m Standard Deviation (MJ m ⁻² day ⁻¹)	1.96	1.53	1.91	1.89	2.72	1.81	2.57
Mean Type Duration (Days)	1.23	1.31	1.59	1.19	1.20	1.33	1.42

1178

1179 **Table 2: Mean daily characteristics and values for each synoptic type.**

1180

1181

1182

1183

1184

1185

1186

1187

1188

1189

1190



1191

	Number of Days	Days with No Cloud Cover	Days with Partial Cloud Cover	Days with Complete Cloud Cover	Days with Any Cloud Cover
Type 1	16	12.50%	43.75%	43.75%	87.50%
Type 2	17	23.53%	52.94%	23.53%	76.47%
Type 3*	46	8.70%	23.91%	65.22%	89.13%
Type 4	19	0.00%	42.11%	57.89%	100.00%
Type 5	24	12.50%	58.33%	29.17%	87.50%
Type 6	16	0.00%	6.25%	93.75%	100.00%
Type 7	34	23.53%	32.35%	44.12%	76.47%

*One day was omitted from classification due to lack of data

1192

1193 **Table 3: Cloud cover characteristics of synoptic types.**

1194

1195

1196

1197

1198

1199

1200

1201

1202

1203

1204

1205

1206

1207

1208

1209

1210



1211

	Number of Days	Percentage of Events
Type 1	16	9.30%
Type 2	17	9.88%
Type 3	46	26.74%
Type 4	19	11.05%
Type 5	24	13.95%
Type 6	16	9.30%
Type 7	34	19.77%

1212

1213 **Table 4: Frequency and percentages of synoptic types.**

1214

1215

1216

1217

1218

1219

1220

1221

1222

1223

1224

1225

1226

1227

1228

1229

1230

1231



1232

1233

From	To						
	T1	T2	T3	T4	T5	T6	T7
T1	0.28	0.22	0.00	0.00	0.06	0.00	0.44
T2	0.12	0.24	0.12	0.12	0.06	0.06	0.29
T3	0.07	0.02	0.39	0.26	0.00	0.22	0.04
T4	0.24	0.29	0.12	0.12	0.12	0.00	0.12
T5	0.00	0.08	0.56	0.04	0.20	0.00	0.12
T6	0.27	0.07	0.07	0.00	0.13	0.20	0.27
T7	0.00	0.24	0.24	0.03	0.42	0.03	0.27

1234

1235 **Table 5: Probability of transition from one synoptic type to another on the following day. Note that T3's most likely**
1236 **transition is to itself (consecutive days of the same synoptic type).**

1237

1238

1239

1240

1241

1242

1243

1244

1245

1246

1247

1248

1249

1250

1251

1252



1253

1254

	Mean	Standard Deviation	Median
Type 1	23	7	23
Type 2	25	6	26
Type 3	24	5	24
Type 4	21	4	21
Type 5	23	4	22
Type 6	17	6	16
Type 7	20	5	21

1255

1256 **Table 6: Statistics on seasonal frequency of synoptic types from 1979 through 2017.**

1257

1258

1259

1260

1261

1262

1263

1264

1265

1266

1267

1268

1269

1270

1271

1272

1273

1274

1275



1276

1277

Phase			Estimated Mean Seasonal Flux (MJ m ⁻²)	No. of Seasons
IOD +	SAM +	-	33.20	16
IOD +	SAM -	-	34.99	11
IOD -	SAM -	-	55.35	6
IOD -	SAM +	-	50.11	6
IOD +	SOI +	-	40.91	12
IOD +	SOI -	-	28.34	15
IOD -	SOI -	-	45.63	2
IOD -	SOI +	-	54.15	10
SAM +	SOI +	-	45.74	13
SAM +	SOI -	-	26.36	9
SAM -	SOI +	-	48.64	9
SAM -	SOI -	-	34.90	8
IOD +	SAM +	SOI +	41.99	7
IOD +	SAM +	SOI -	26.36	9
IOD +	SAM -	SOI +	39.39	5
IOD +	SAM -	SOI -	31.32	6
IOD -	SAM +	SOI +	50.11	6
IOD -	SAM +	SOI -	0.00	0
IOD -	SAM -	SOI +	60.21	4
IOD -	SAM -	SOI -	45.63	2

1278

1279 **Table 7: Mean seasonal snowpack energy flux values associated with various IOD, SAM, and SOI phase combinations.**

1280

1281

1282

1283

1284

1285

1286